ELECTROSTATIC ION-ION TWO-STREAMING INSTABILITY IN A THERMAL-BARRIER CELL

by

V. A. Thomas and W. M. Nevins

Memorandum No. UCB/ERL M84/22

22 February 1984

ELECTRONICS RESEARCH LABORATORY

College of Engineering
University of California, Berkeley
94720

Electrostatic Ion-Ion Two-Streaming Instability In a Thermal-Barrier Cell

V. A. Thomas

Electronics Research Laboratory, University of California,
Berkeley, California 94720

W. M. Nevins

Lawrence Livermore National Laboratory, University of California,
Livermore, California 94550

ABSTRACT

Some designs for tandem mirror devices rely on a thermal-barrier cell, a region of depressed potential located between the central cell and the end plugs. This region of depressed potential relies on, to some extent, an ion distribution function that has two peaks in v_z (ion velocity parallel to the magnetic axis). Therefore there is a possibility that some ion-ion two-stream modes can be unstable. Using 1-d models, the stability of model equilibria to electrostatic ion two-stream modes is considered. Our results suggest that for parameters of greatest interest (i.e., for planned experiments), these modes should be stable. Particle simulation techniques are used to examine the nonlinear consequences for those conditions where instability is present.

February 22, 1984

Electrostatic Ion-Ion Two-Streaming Instability In a Thermal-Barrier Cell

V. A. Thomas

Electronics Research Laboratory, University of California,

Berkeley, California 94720

W. M. Nevins

Lawrence Livermore National Laboratory, University of California,

Livermore, California 94550

1. Introduction

Many previous papers have been devoted to the study of electrostatic ion-ion streaming instabilities: Foote and Kulsrud[1] , Perkins[2] , Weibel[3] , Forslund and Shonk[4], and Stringer[5] among others. In particular, Lontano, Pekker and Pozzolli[6] examined the possibility of electrostatic ion-ion two-steam modes occurring in the a thermal-barrier cell of a tandem mirror. They concluded that instability is likely under conditions of interest in proposed and actual experiments. However their pessimistic conclusion may result primarily from their choice of a thermal-barrier ion distribution function that has no trapped ions in the combined electrostatic and magnetic potential well of the thermal-barrier cell.

In this paper use is made of ion distribution functions which realistically include thermal-barrier trapped-ions. These distribution functions were first constructed by Cohen[7] and were designed to model results from recent Fokker-Planck computer simulations of the time independent equilibria of thermal-barrier cells; these analytic models were used by Cohen to calculate the self-consistent axial electrostatic fields in a thermal-barrier cell equilibrium. In this paper we will first make use of Cohen's model distribution function and his equilibrium fields

to examine their stability using infinite medium theory. Complementary 1-d particle simulations will then be done using these ion distribution functions, first in a periodic homogeneous model and then in a novel inhomogeneous model. Results from both our stability analysis and from our simulations imply an optimistic view of the stability properties of realistic thermal-barrier cells (e.g., TMX-U and MFTF-B) to the electrostatic ion-ion two-stream modes.

2. The Time Independent Equilibrium

The thermal-barrier concept as part of a tandem mirror is basically a potential depression located in a magnetic mirror between the central cell and the end plugs; it serves to isolate the electron populations in the two regions. A schematic diagram of one possible design is shown in Fig. 1; a detailed description of the original thermal-barrier concept is given in Baldwin and Logan[8]. The thermal-barrier makes it possible to achieve a large confining potential for the tandem-mirror central cell ions, using only a relatively low plasma density in the plug region. This potential depression is created in part by the removal of any ions which might be trapped in the thermal-barrier. With no trapped-ions inside the thermal-barrier cell, the ion distribution function at the magnetic field minimum is double-peaked in parallel velocity, and the ion density there is correspondingly depressed. The thermal-barrier equilibrium is sometimes described as an ion-hole type of solitary potential structure; however it is unlike most ion-holes in that it is many Debye lengths long.

Equilibrium studies of the thermal-barrier cell are useful in order to gain an understanding of the microstability properties of the cell. Self-consistent equilibrium solutions allow one to estimate the particle density and the velocity distributions as functions of position. One may then analyze the stability as a function of the resulting equilibrium parameters. It should be realized, however, that our self-consistent equilibria are generated using Cohen's model distribution functions and as such may be in error if the equilibria are heavily model dependent. To determine how model dependent our results are, equilibria have also been studied using a different kinetic ion model from Cummins[10], as detailed in Appendix A.

The equilibrium axial electrostatic fields are solved for by assuming model distributions

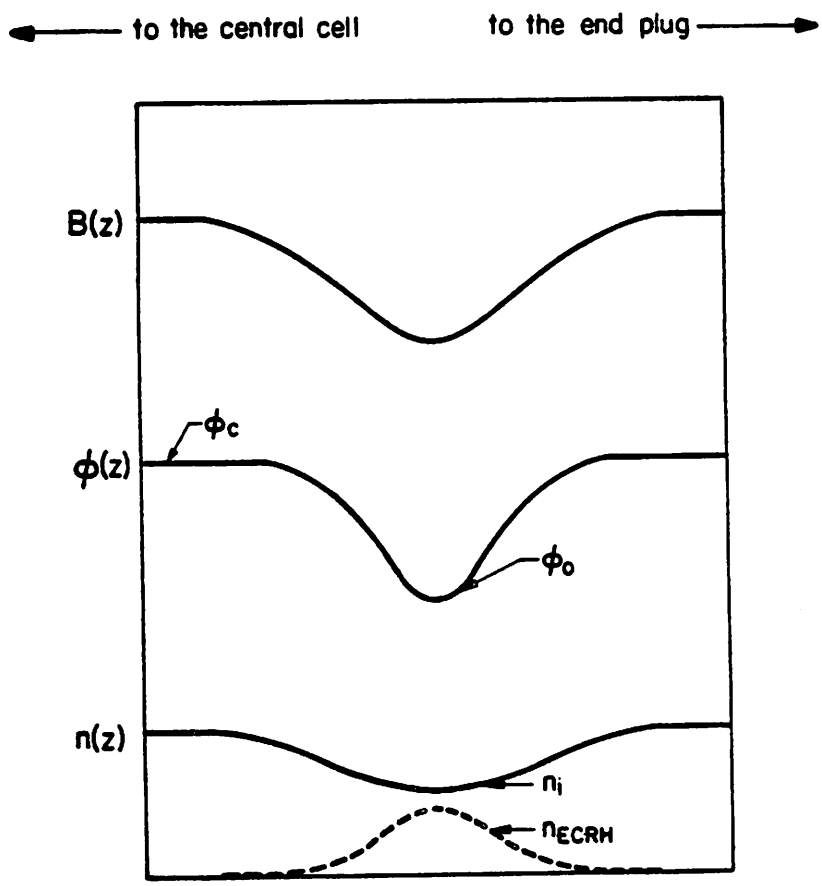

FIG. 1. Schematic axial potential profile for a thermal-barrier. Here ϕ_c is the central cell potential and ϕ_0 is the potential of the minimum in the thermal-barrier cell . The quantity n_{ECRH} represents the energetic mirror trapped electrons due to the applied electron cyclotron resonance heating.

for the ion and the electron populations. These model distribution functions are expressible in terms of the constants of motion since they are used for equilibrium calculations. In general the constants of the motion are not limited to the energy and the magnetic moment of the particles. The distribution function may have multiple sheets representing the different trapped populations which are not in contact with each other. This is analogous to the famous case of BGK modes[9] where the trapped particle distribution may depend upon which region the trapped particles are in. These possibilities will not be included in this paper.

The ion population is modeled as consisting of two groups, the thermal ions and the sloshing ions. The thermal ion distribution consists of those ions *passing* freely between the central cell and the thermal-barrier region, and those central-cell ions which have been *trapped* by collisions in the thermal-barrier cell. The sloshing ions have been included in some thermal-barrier designs and consist of energetic ions confined entirely by the magnetic well. These ions are to be generated by injection of neutral beams. In this paper we will not go into the details of the sloshing ion distribution function, even though these details can be important for determining the potential profile in the thermal-barrier cell. The primary aim of this paper is to examine the stability of likely thermal-barrier distribution functions; thus for our purposes, also considering sloshing ions amounts simply to considering an ion distribution that is more double peaked (in parallel velocity space) at the magnetic field minumun.

The model distribution function for the thermal ions as developed by Cohen[7] can be expressed in terms of the invariants μ and ϵ , where μ is the magnetic moment for the ion and ϵ is the ion kinetic energy. In this model the passing ion component is assumed to have a Maxwellian distribution, while the ions trapped in the thermal-barrier cell are given the distribution

$$f_{trapped} = n_0 \left(\frac{m_i}{2\pi T_i}\right)^{3/2} \exp\frac{(\epsilon - \alpha B_{max}\mu)}{(\alpha - 1)T_i} \qquad (1)$$

where B_{max} is the magnetic field strength at the mirror throat and T_i is the ion central cell temperature. The quantity α is an artificial parameter which is always kept greater than one; varying α controls the relative density of trapped and passing ions. The limit value $\alpha = 1$ defines a

thermal ion distribution with *no* trapped ions; raising the value of α from unity increases the relative density of trapped ions to passing ions.

The electron population is also modeled as composed of two different groups, the energetic (ECRH) electrons and the thermal electrons. The ECRH population is assumed to respond only to the magnetic field and as such is independent of the electrostatic potential, $\phi(z)$; the less energetic thermal electron population is modeled as a massless fluid with a spatially uniform temperature, T_e, whose density n_{th} responds only to electrostatic potential. The reader is referred to Pearlstein and Nevins[11] for a more complete electron model.

Using a given electron response, the self consistent solution for the axial electrostatic fields is found by imposing the quasineutrality condition:

$$n_e(\phi,B) = n_{ECRH}(B) + n_{th}(\phi) = n_i(\phi,B) \quad . \tag{2}$$

In performing these calculations it is necessary to choose a form for the magnetic field as a function of the axial coordinate, $B(z)$. Different equilibria are obtained by varying the parameters T_e/T_i , α , n_{ECRH} and $B(z)$. The quasineutral solutions $\phi(z)$ are smooth functions over much of the range of the parameter space for these variables providing that $L \gg \lambda_D$ where L is the length of the thermal-barrier cell; this is quite valid for several systems of interest. However under some conditions, the equilibrium solutions may develop sheaths (when the trapped ion density is very small, or for those cases where the energetic electron population has too large a density). An example of a smooth self-consistent axial potential profile is presented in Fig. 2.

The parameters α, T_e/T_i, and n_{ECRH} are important parameters in determining the appearance of the equilibrium solution. Physically, it is required that the potential dip in the thermal-barrier cell be sufficient to inhibit thermal contact between the central cell and end cell electron populations. Adequate thermal-barrier model equilibria can be constructed either having mostly passing ions and very few trapped ions (small α), or having relatively more trapped ions; but these two extremes (i.e., model equilibria having large and small α) must be considered quite differently. A thermal-barrier equilibrium having few trapped ions has a larger ion

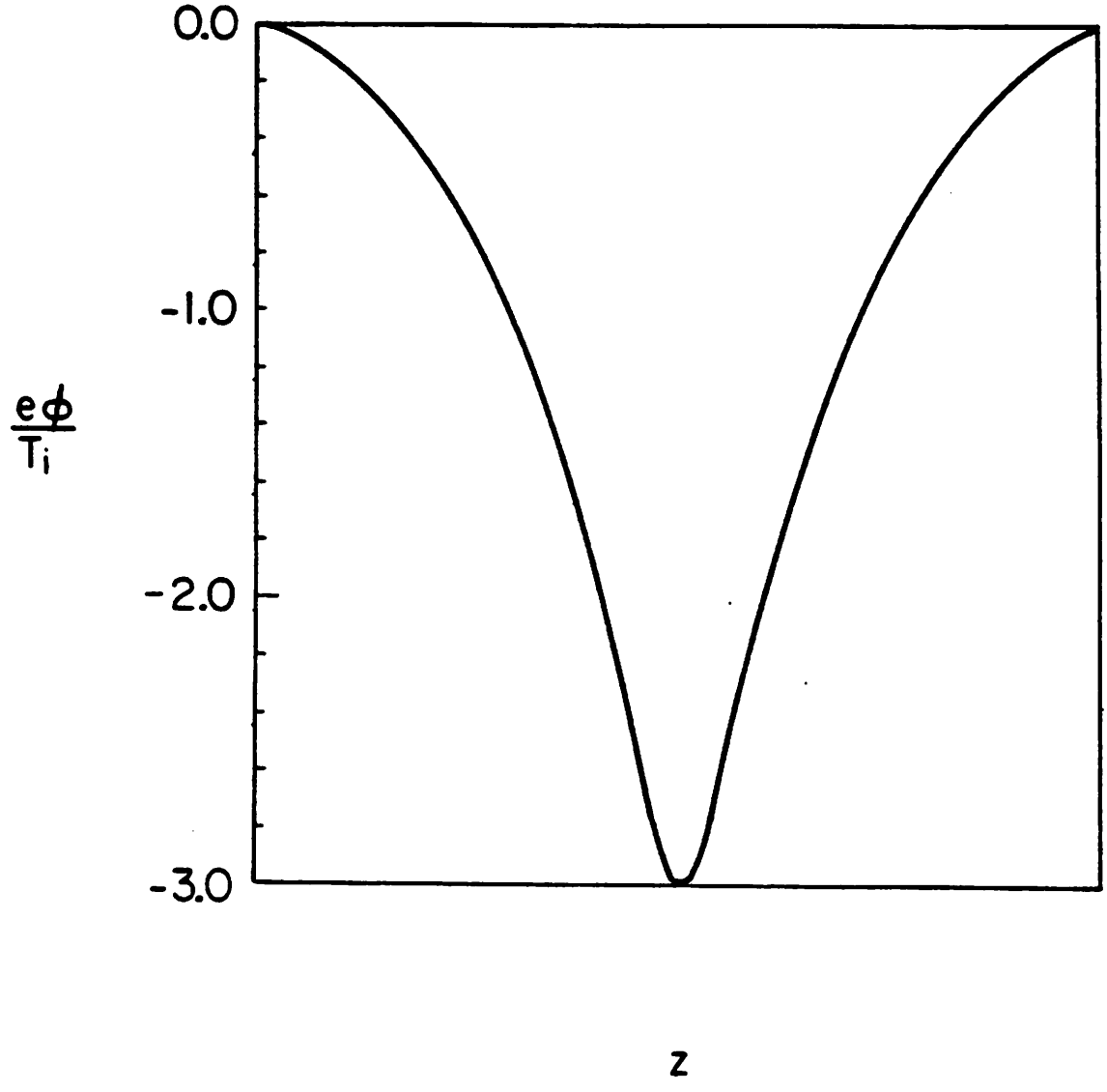

FIG. 2. Axial potential profile for $\alpha = 4.0$. Here $n_{ECRH} = const\left[(1-1/R)/(1-1/R_M)\right]^{3/2}$ where R is the local mirror ratio and R_M is the maximum local mirror ratio in the system which for this problem is 3 . The axial magnetic field is given the form $B(z) = B_{max} - A\sin(\frac{2\pi z}{L})$ with L being the length of the system. The central cell ion and electron temperatures are equal. The minimum ion density is 0.43 of the maximum density. The filling parameter g may be obtained from Fig. 7.

density depression at the magnetic field minimum than does an equilibrium with many trapped ions; it turns out that for smaller values of α, pumping out the barrier-trapped ions alone is sufficient to generate the required potential dip. For large values of α, the ion density at the magnetic field minimum increases and it becomes necessary to include a significant number of energetic (ECRH) electrons to establish the desired potential depression.

It turns out that the functional form of this energetic electron component as a function of $B(z)$ is important in determining the stability of the electrostatic ion-ion two-stream mode. Since this energetic electron component is formed by applying ECRH away from the magnetic field minimum, their density $n_{ECRH}(z)$ must be double peaked initially with the peaks occurring at the turning points of the energetic electrons. However, as indicated in Poulsen[12] the dominant collisional processes are pitch angle scattering and drag, implying that the asymptotic energetic electron spatial distribution has only one local maximum located at the magnetic field minimum. On the other hand, during start-up the energetic electrons will have two spatial maxima. This start-up period is quite long compared to the time scale for instabilities since the energetic electrons are at least weakly relativistic and therfore have quite long collision times. Therefore we need to examine equilibria that have ECRH electrons having one and two spatial maxima.

As a check of the numerical solutions " test ion " particle simulations were performed, using a simulation model described in section 5. Initially the ions were loaded with their equilibrium parameters. Then keeping the axial electric field fixed at its equilibrium value, the ions were advanced for a time equivalent to many bounce periods of a typical trapped ion. The effect of the nonuniform magnetic field was modeled by using a $\mu \nabla B$ force. The ion density and the ion velocity distribution function were monitored as a function of space and time. In addition, the self consistent axial potential was computed from the particle positions and compared to the equilibrium axial potential. The self-consistent potential fluctuated about the equilibrium potential profile due to the finite number of simulation particles. These diagnotics verified that a physically realistic equilibrium had been obtained. We mention that the particle

density weighting had to be made proportional to the local magnetic field strength, to account for the flux tube expansion (pointed out to us by Byers[13]).

3. Linear Theory

In this section we review the kinetic, Vlasov-Poisson linear theory for the ion-ion electrostatic two-stream instability in an infinite uniform medium for the restricted case where the wavevector is parallel to the magnetic field. The theory is then applied to the thermal-barrier cell.

As mentioned in the introduction, similar studies have been performed previously including propagation at an angle to the magnetic field. Our results are different in that we use a different model distribution function for the ions, ours being more appropriate for the thermal-barrier cells than the earlier models. As it turns out, for parameters likely to occur in thermal-barrier cells our model distribution function is more stable than both the ion distribution function in Lontano, Pekker and Pozzolli[6] (who have no trapped ions) and the counter-streaming Maxwellian ion distribution function of Foote and Kulsrud[1]. We also present a detailed pictorial account of the relevant quantities of interest for this instability.

3.A: Solutions to the Dispersion Relation

The appropriate dispersion relation for our analysis is given by $D(\omega,k) = 0$ with

$$D(\omega,k) = -1 - \frac{1}{k^2\lambda_{De}{}^2} + \left(\frac{1}{k^2\lambda_{Di}{}^2}\right)\int \frac{\frac{df(v_z)}{dv_z}}{v_z - \frac{\omega}{k}}dv_z \tag{3}$$

where v_z is the parallel velocity and the reduced distribution function is normalized to unity. The quantity λ_{De} represents the linear electron response and may be used to define an effective electron temperature. This effective electron temperature, $T_{e\,eff.}$, is calculated in the general case by using

$$\chi_e = -\frac{4\pi}{k^2}\left(\frac{\delta\rho_e}{\delta\phi}\right) \equiv -\frac{4\pi}{k^2}\left(\frac{n_e q_e^2}{T_{e\,eff.}\, m_e}\right) \equiv \frac{1}{k^2\lambda_{De}^2} \quad . \tag{4}$$

For an electron distribution which is a sum of Maxwellians of different temperatures one may

write

$$T_{eff.}^{-1} = \sum_s \eta_s \, T_s^{-1} \tag{5}$$

where η_s is the fraction of the s^{th} component. Hence, shielding is likely to be dominated by the cooler component. Note that the imaginary portion of the electron susceptibility is being ignored. This eliminates the possibility of resonant electron instabilities.

Nyquist analysis is useful to illuminate some of the characteristics of the instability. The Nyquist technique requires that the dispersion function be be mapped from a contour just above the real axis in the complex ω plane. The number of times the origin in the complex D plane is encircled by this contour is equal to the number of unstable roots in the system. The function $D(\omega,k)$ is defined by Eq. (3).

First, we note that our ion distribution function is bimodal and is symmetric about the origin. Therefore $\mathrm{Im}\left[D(\omega,k)\right]$ is equal to zero only at five points along our contour just above the real axis in the complex ω plane. These points satisfy $df(v_z)/dv_z = 0$ and therefore the residue is equal to zero. These points are given by $\omega = \pm\infty$, $\omega = 0$, and $\omega = \pm k\, v_{\max}$ where $v_{\max}$ is the ion velocity at the maximum in the distribution function for parallel velocities. The values of $\mathrm{Re}\left[D(\omega)\right]$ at the frequencies where $\mathrm{Im}\left[D(\omega)\right] = 0$ are

$$RD_1 = -\left[1 + \frac{1}{k^2\lambda_{De}{}^2}\right] \quad , \quad RD_2 = -\left[1 + \frac{1}{k^2\lambda_{De}{}^2}\right] + \left[\frac{1}{k^2\lambda_{Di}{}^2}\right] \int \frac{\dfrac{df(v_z)}{dv_z}}{v_z} \, dv_z \quad ,$$

and

$$RD_3 = -\left[1 + \frac{1}{k^2\lambda_{De}{}^2}\right] + \left[\frac{1}{k^2\lambda_{Di}{}^2}\right] \int \frac{\dfrac{df(v_z)}{dv_z}}{v_z - v_{\max}} \, dv_z$$

respectively. All of these values are less than zero ($RD_{1,2,3} < 0$) with the possible exception of the value at $\omega = 0$. This behavior is shown in the schematic Nyquist diagram for this problem in Fig. 3. Therefore there is at most one unstable root to the dispersion relation. We also see that at marginal stability the frequency is given by $\omega = 0$. This just implies that the path in the complex D plane goes through the origin. In addition we may conclude that the instability has

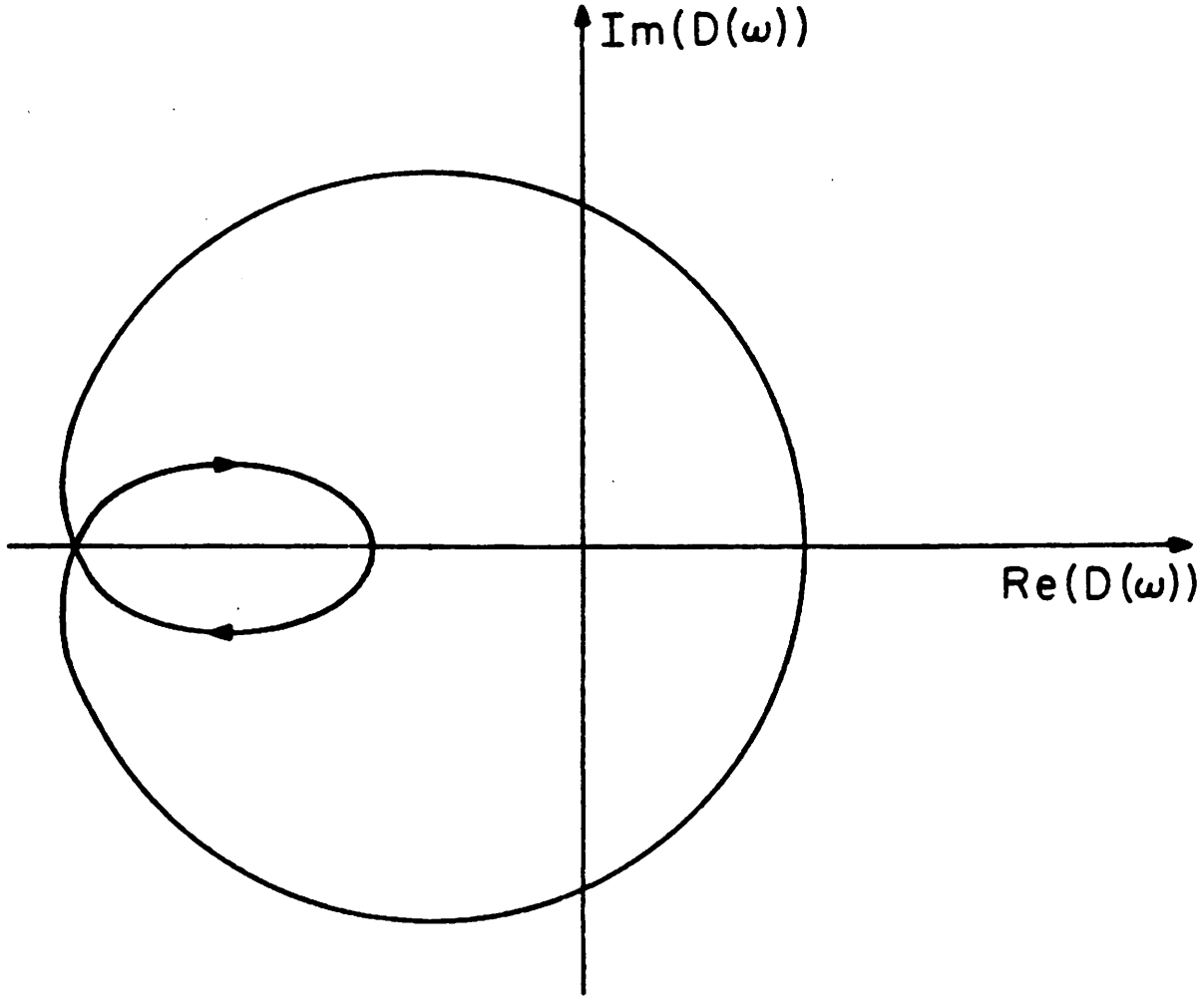

FIG. 3. Schematic Nyquist diagram for our problem. This diagram indicates one unstable mode since the origin in enclosed one time.

$\omega_r = 0$. This follows from the fact that $\omega = \omega_r + i\gamma$ and $\omega = -\omega_r + i\gamma$ are both solutions to the dispersion relation. The existence of only one unstable root forces ω_r to be equal to zero.

In addition to solving for marginal stability, it is of general interest to solve the dispersion relation to find the maximum growth rates and the wavelengths of the unstable mode as functions of the characteristic parameters of the system. In particular, it is interesting to show γ_{max} and the corresponding wavelength for fixed α in a plane, with the x axis representing the normalized drift velocity and the y axis representing the temperature ratio $T_i/T_{e\ eff.}$. The normalized drift velocity, u, is defined as $(-2e\delta\phi/T_i)^{1/2}$ where $\delta\phi$ represents the negative potential difference between the location in the thermal-barrier cell and the central cell of the tandem mirror. These detailed calculations are summerized in Fig. 4 only for the model ion distribution function from *Cohen*[7].

In Fig. 4 contour plots for γ_{max} and the corresponding wavelength for a particular value of the parameter α are shown. The growth rate is a relatively insensitive function of k near its maximum and so the contours for k are not too smooth. A representative plot of γ vs k for a point in the $(u, T_i/T_{e\ eff.})$ plane is given in Fig. 8. An important feature is the fact that near marginal stability the quantity γ_{max} is a relatively slowly varying function of the effective electron temperature. This implies that a system becoming unstable because of some kind of fluctuation is likely to be unstable with a small growth rate. As will be discussed in the simulation section, a small growth rate leads to low saturation levels for the perturbed field quantities. It is also to important to note that the wavelength corresponding to the most unstable mode is considerably longer than the ion Debye length over much of the unstable parameter space. This suggests that finite length effects could become important in that the most unstable wavelength may not be negligible compared to the characteristic length of the system. Had the most unstable wavelength been equal to the ion Debye length finite length effects could be expected to be very small.

It should be pointed out here that the fact that the contours reach a maximum value of $T_i/T_{e\ eff.}$ and then turn back down toward the x axis as the drift velocity is increased is an

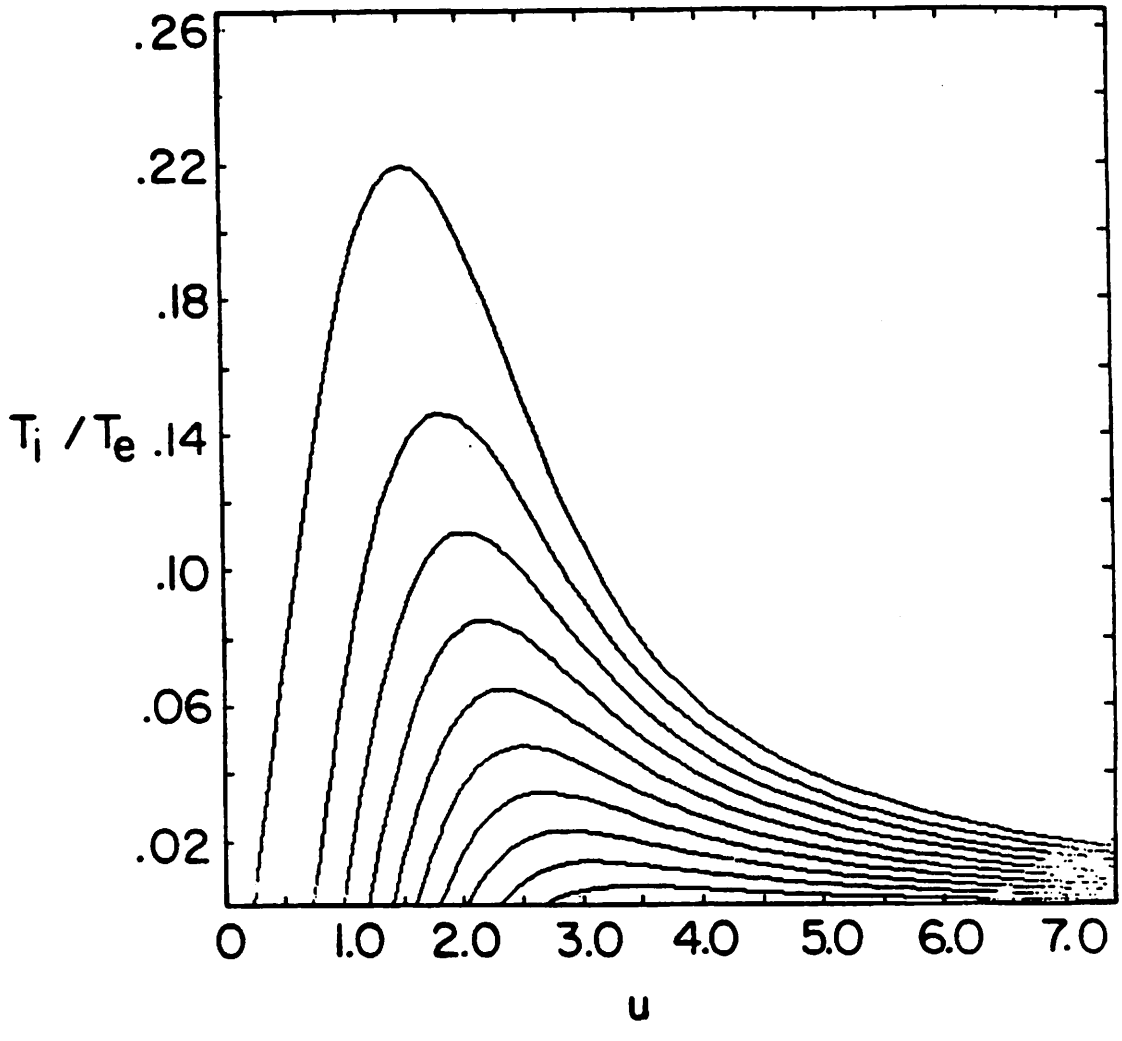

FIG. 4. Contour plots showing (a) maximum growth rates and (b) the value of $k\lambda_{Di}$ corresponding to that maximum growth rate. The local mirror ratio is $rb = 3$ and the parameter α is equal to 1.9 . The contours of growth rate are spaced $0.034\omega_{pi}$ apart and the contours of $k\lambda_{Di}$ are 0.025 apart. The wavelength is infinite at marginal stability , the outer most curve. The quantity u is the normalized drift velocity as described in the text.

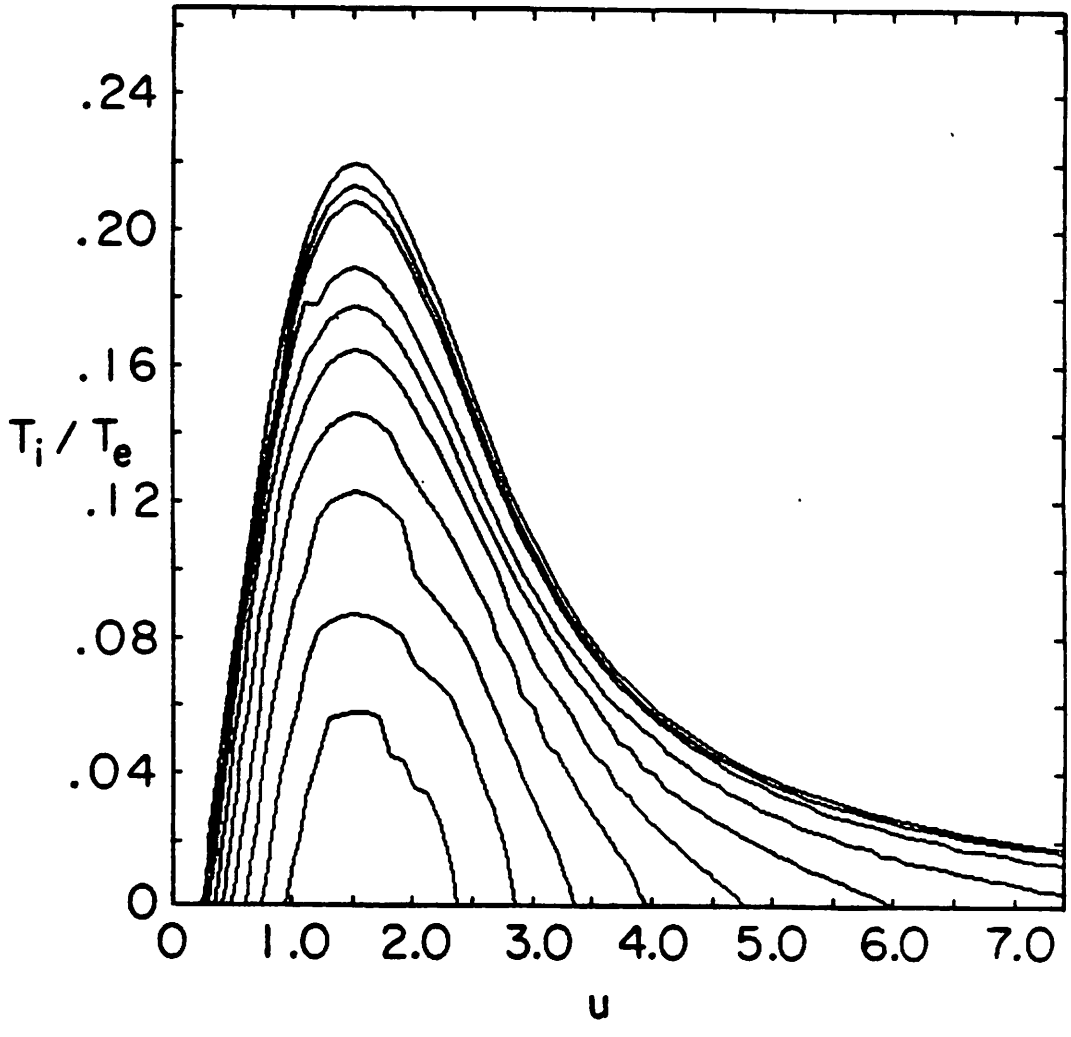

FIG. 4b.

artifact of including only wavevectors parallel to the magnetic field. If off- axis propagation is allowed then the growth rate contours will not come down from their value at the maximum $T_i/T_{e\ eff.}$ as the drift velocity is increased. Rather, the the wavevector will move off axis so that the drift velocity parallel to the wavevector is reduced. Then, assuming that the addition of the perpendicular wavevector component does not alter the physics of this zero frequency mode (i.e. the growth rate is larger than the ion cyclotron frequency) , the growth rate contours will reach a maximum value of $T_i/T_{e\ eff.}$ and then remain at that value as the drift velocity is increased.

Foote and Kulsrud[1] have shown that this type of unmagnetized zero frequency mode is the most unstable mode for counter streaming Maxwellian ion beams until the drift velocity reaches twice the value at which the growth rate of the parallel propagating mode begins to decrease. For larger drift velocites an ion cyclotron instability is the most unstable mode.

The preceeding plots are all for a particular value of the parameter α. For larger values of the parameter α, the trapped ion component increases for a fixed value of $\delta\phi$. The major effect of this change is to shift the contour plots along the x axis and to compress them in the y direction. The general shape of the maximum growth rate contours remains the same. The maximum growth rate also does not vary much. On the other hand the wavelength corresponding to the most unstable mode increases. These general characteristics are evident in Fig. 5. This is qualitatively easy to understand since the effective ion temperature is given by the width of the distribution function in v_z and not by the quantity T_i (which represents the central cell ion temperature) .

The marginal stability diagram in Fig. 6 (a) is also indicative of this " similarity " in the nature of the distribution function as the parameter α is varied. This figure gives contours of marginal stability for fixed $T_i/T_{e\ eff.}$ in the $(\alpha, e\delta\phi/T_i)$ plane. For a given contour line the system is unstable between that line and the ordinate. For this instability the relevant boundary is that at smaller values of the drift velocity since for larger drift velocities the parallel propagating mode may not be the most unstable mode. For drifts larger than the lower boundary of a

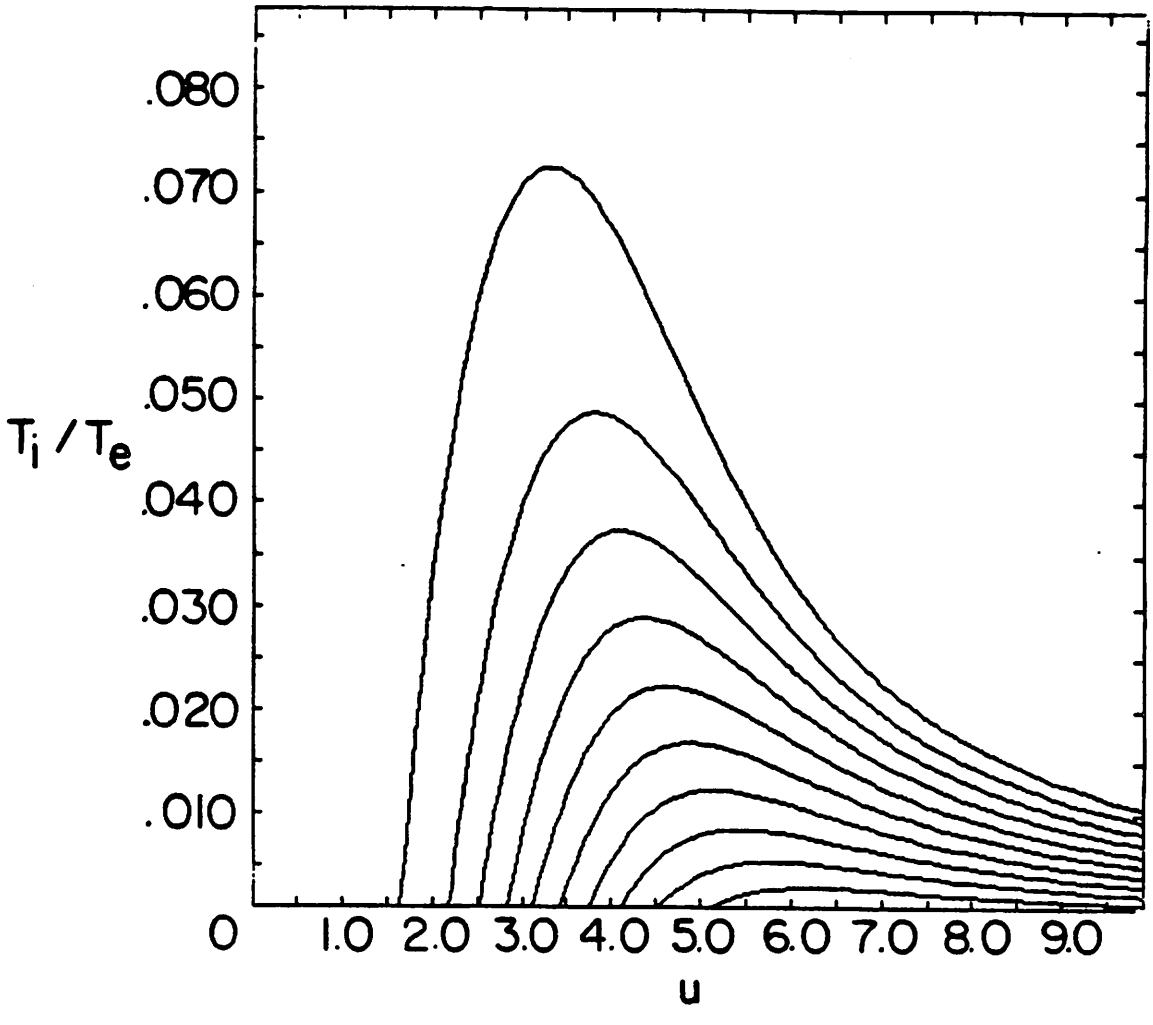

FIG. 5. Contour plots of (a) maximum growth rate and (b) value of $k\lambda_{Di}$ corresponding to the maximum growth rate. The parameter $\alpha = 4.0$ and the other parameters are the same as in Fig. 4 except that now the contours of $k\lambda_{Di}$ represent 0.0145 and the contours of γ_{max} represent $0.0327\omega_{pi}$.

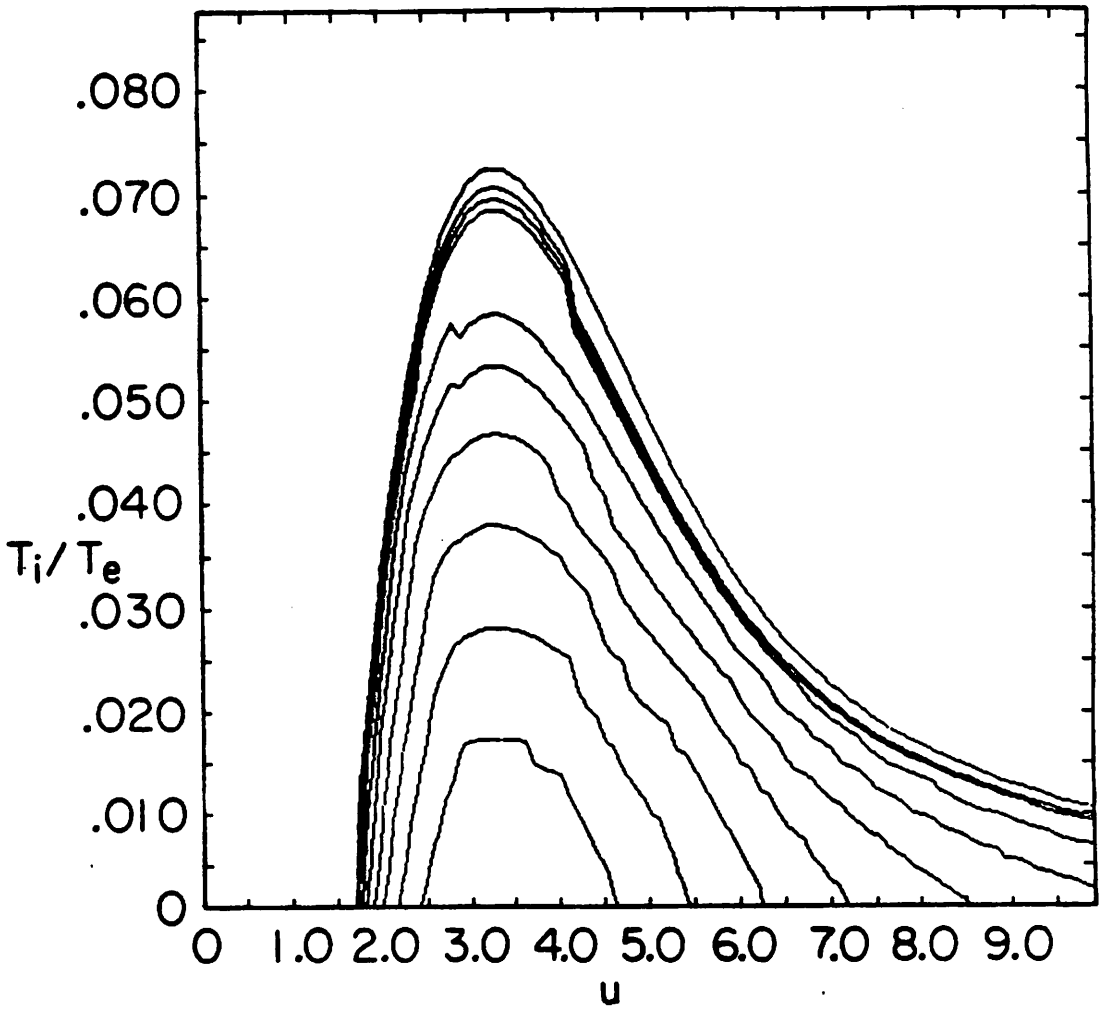

FIG. 5b.

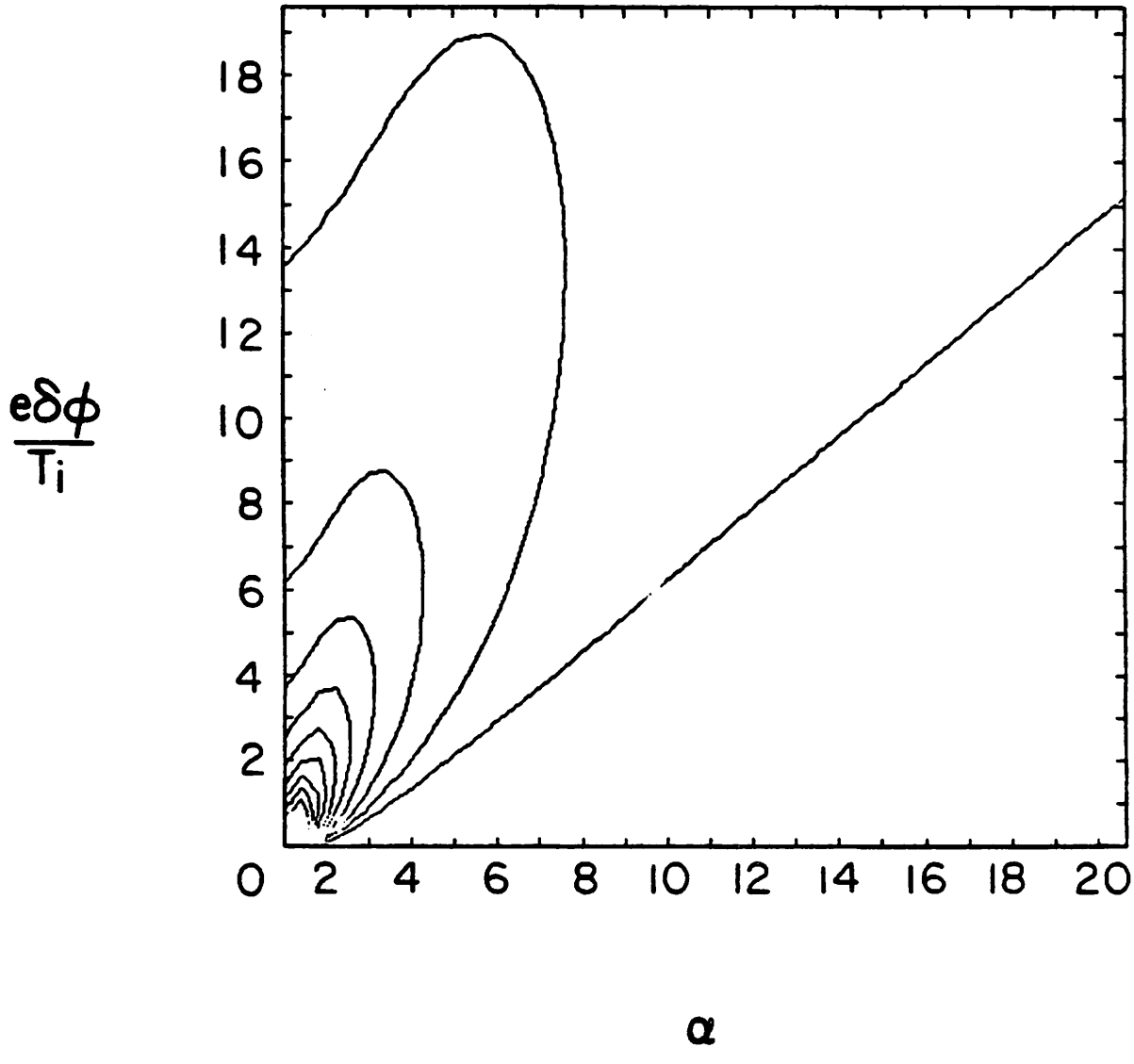

FIG. 6. Contours of (a) marginal stability for fixed effective electron temperature and (b) the quantity $g = n_{total}/n_{passing}$ in the $(\alpha, e\delta\phi/T_i)$ plane. The contour that extends furthest to the right in (a) represents an infinite effective electron temperature. The other contours are equally spaced with increments $T_i/T_{e\,eff.}$ of 0.03. Contours with $T_i/T_{e\,eff.}$ greater than 0.30 are not shown to facilitate viewing. The contours actually extend to $T_e = T_i$ for very small values of the parameter g. Contours in (b) are in intervals of 2 starting with $g = 2$ and ending with $g = 22$. The mirror ratio is $rb = 3$.

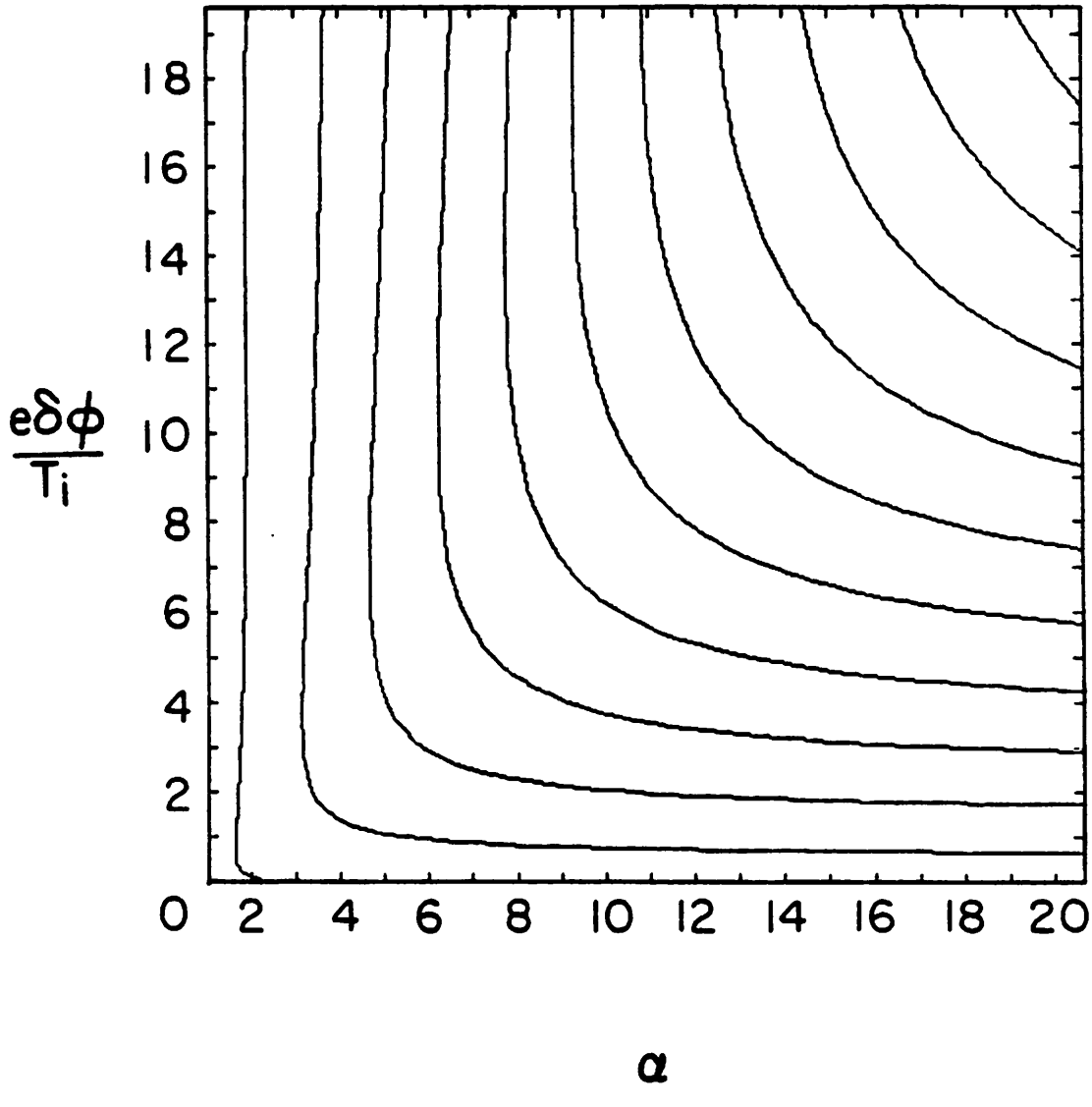

FIG. 6b.

given curve, the zero frequency instability will exist at some angle to the magnetic field as discussed above.

Figure 6 (b) shows the quantity $g = n_{total}/n_{passing}$ in the same plane. Here n_{total} is the total ion density and $n_{passing}$ is the passing ion density. Thus g gives an indication of the pumping required to be located at a point in our marginal stability plane. The local mirror ratio $B(z)/B_{max}$ plays only a small part in the positions of these lines as long as it is not too close to unity. For very small values of g the system is unstable at relatively low $T_{e\ eff.}/T_i$ and at low drift velocities. This corresponds to the results of Ref. 6 where $g = 1$. These parameters are not of interest to an actual experiment because trapped particles will exist in any experiment.

In Fig. 7 the corresponding marginal stability plots for the ion distribution function from Cummins[10]are shown. It is seen that for a given value of g this distribution function is more unstable than the previous one. As the parameter g approaches unity the stability boundaries for the two models also approach each other, as must happen.

3.B: Applications to Thermal-Barriers Cells

An indication of the stability of the thermal-barrier cell can be obtained by considering the cell minimum. At that point the ion distribution function has its most extreme (counter streaming)form, and the electron shielding is the weakest and therefore maximum instability is expected. The stabilizing electron shielding response may be due mostly to the small density of electrons at the central cell temperature. Residual shielding due to the energetic electrons may become important if the density of central cell electrons is very low.

Thermal-barriers for positive operation of a tandem mirror operate in the range of $e\delta\phi/T_i$ on the order of three to four. Here $\delta\phi$ represents the potential drop between the central cell and the minimum of the thermal-barrier cell. At the present time the best estimates for the parameter g in planned experiments range from $g = 5.0$ to $g = 6.0$. The marginal stability plots show that instability is possible for parameters in these ranges depending upon the effective electron temperature.

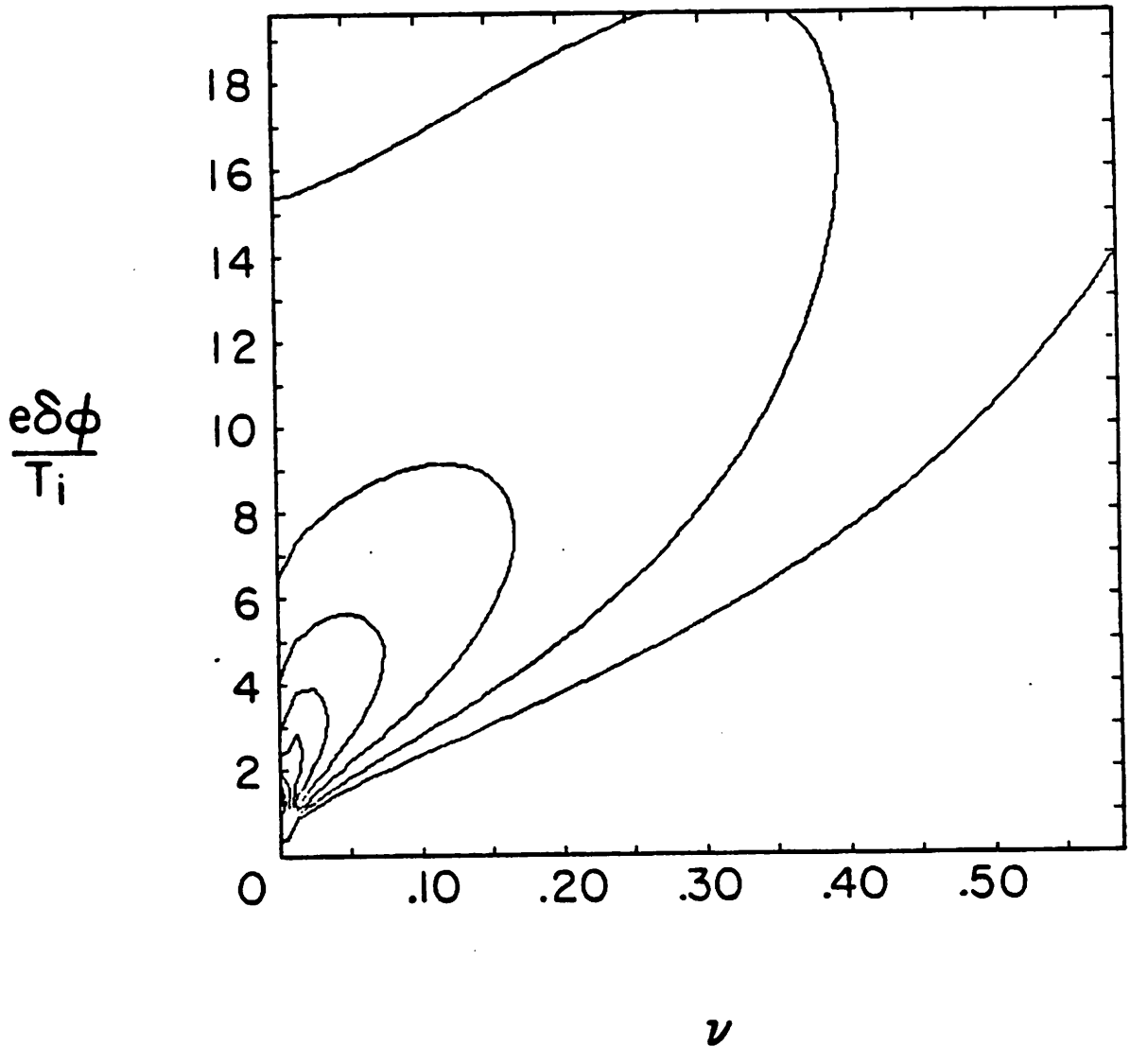

FIG. 7. Contours of (a) marginal stability for fixed effective electron temperature and (b) the quantity g in the $(\nu, e\delta\phi/T_i)$ plane. The quantity ν is defined in Appendix A. The contour intervals are the same as in Fig. 7. The first contour on the left in (b) represents $g = 2$.

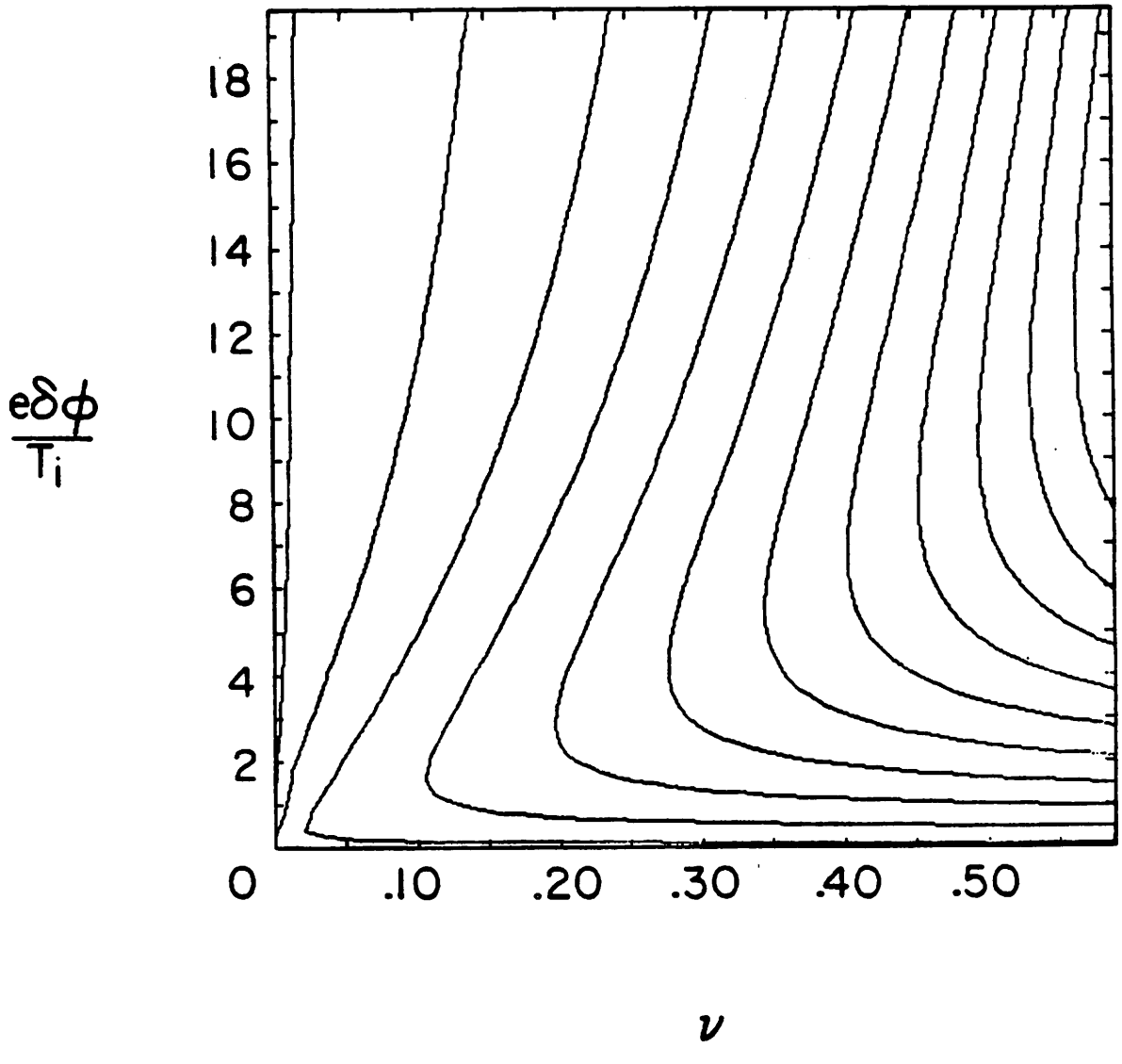

FIG. 7b.

For the negative operation of a tandem mirror the quantity $\delta\phi$ needs to be significantly larger than for the positive mode of operation. This increase is to make the end loss of the central cell ions initially larger than the end loss for the central cell electrons which means that the potential of the device would be driven negative with respect to ground in order to enforce ambipolar end losses. Another factor that needs to be considered is that at the edge of the thermal-barrier cell (i.e. closest to the wall) there are essentially no thermal electrons . The entire electron distribution there consists only of ECRH magnetically confined electrons. The effective temperature of these electrons could be on the order of one hundred times the ion temperature. The range of $e\delta\phi/T_i$ is from about six to twenty. For this situation the values of g must be much larger than for the positive mode in order to achieve stability. The reader is referred to Poulsen et. al.[12] for a detailed description of the negative operation of the thermal barrier concept.

From a systematic examination of the self consistent equilibria we have obtained the general characteristics of the unstable equilibria. First, for a fixed potential drop, equilibria with cooler electrons are more unstable than equilibria with warmer electrons. This is due to the fact that the electron shielding term is weaker at the cell minimum for the cooler electrons due to the exponentially decreasing density. The equilibria for these cases have a double peaked electron density in space. This is necessary because the thermal electron density is much smaller than the ion density near the well center. Therefore the ECRH component must be almost equal to the ion density near the potential minimum. The ion density falls near the potential minimum and so the ECRH electron component must also have a local minimum at that point. Unstable equilibria also exist with T_e/T_i greater than one. Again the most unstable equilibria have ECRH electrons with two maxima along the axial direction. Second, both models yielded similar results for equal values of trapped ions. Hence these general features appear not to be too model dependent.

Given the fact that unstable equilibria exist, it is important to understand the nonlinear consequences of the instability and its implications for operation of thermal-barrier cells. This

question will be explored in the simulation sections that follow.

Finally , we would like to discuss briefly four other relevant points. First, our treatment only includes the thermal ions. The sloshing ion component can make the ion distribution function more double peaked. Also our approach is based upon a model for the thermal ions and this model may not be sufficiently accurate. However, our stability analysis has shown that the desired potential profiles can be achieved with distribution functions that are stable to the electrostatic ion-ion two-stream mode.

Secondly, our treatment only considers parallel propagation of the electrostatic ion-ion two-stream mode. However, in analogy to previous papers (Foote and Kulsrud[1] and others), the parallel propagating mode is the first mode which may become unstable as the drift velocity of two beams becomes greater and greater. The parallel propagating mode is also the first mode which may become unstable as the distribution function becomes more and more depleted in the trapped region of phase space. Thus the parallel propagating mode should be the most unstable mode for thermal-barrier cells that have a high proportion of trapped ions.

Thirdly, unstable electromagnetic modes might be possible, as discussed in Foote and Kulsrud[1]. Their work was for Maxwellian beams and so application of their results directly to this problem is not justified.

Lastly, there is a possibility for the radial nonuniformities in the plasma to cause instability. For example, there may be coupling between ion beam modes and drift waves. This problem is currently being considered.

4. Particle Simulations in the Spatially Uniform Limit

In this section results are presented from 1-d electrostatic particle simulations in a uniform plasma. The aim of these simulations is to obtain a scaling law for the perturbed potential at saturation and the final shape of the ion distribution function $f_i(v_z)$ for instabilities that can be considered localized. In particular it is of interest to examine under what conditions the particle distribution function relaxes back to marginal stability. These 1-d simulations are also to be used for comparison with the axially nonuniform simulation which are in the following

section.

Previous particle simulations of electrostatic ion-ion two-stream modes were performed by , among others , Forslund and Shonk[4] for the case of interpenetrating Maxwellian plasmas where the drift velocity was large compared to the ion thermal speed. Their simulations were two dimensional in order to include the most unstable modes (which had wave vector almost perpendicular to the directed ion motion). Their simulation model included both particle ions and particle electrons (where the electrons had an artificially large mass). Our simulations are of a different limit, namely the regime where the ion thermal speed is comparable to the drift velocity. For our case the most unstable modes have their wavevector along the magnetic field or at a small angle to the magnetic field and so may be examined with a 1-d unmagnitized model. For example see Foote and Kulsrud[1].

4.A: Simulation Model

The simulation model is periodic and is spatially uniform initially. The ions are treated as fully nonlinear particles and the electrons are treated as a massless fluid with a Boltzmann response together with a fixed negative charge density representing the energetic electrons. The field solve consists of solving the equation

$$\nabla^2 \phi = e\left(- n_i + n_e \exp\left(\frac{e\phi}{T_e}\right) + n_{ECRH}\right) \quad . \tag{6}$$

The field solve is based upon an iterative approach as in Mason[14] and is described in Appendix B. The ion density n_i is collected on the grid using standard linear weighting; the ECRH electron density component is fixed throughout the simulation. The simulation model gives good agreement with theory as shown in Fig. 8. In performing these simulations only one Fourier mode was retained while advancing the particles; this eliminates possible nonlinear effects between the modes and allows easier evaluation of the performance of the code.

We present one collection of simulations that are indicative of the behavior of the instability. Our parameters are: $\alpha = 4$, $rb = 3$, and $e\delta\phi/T_i = 5$. Here rb represents the local mirror ratio which is defined as the ratio of the magnitude of the axial magnetic field at the mirror

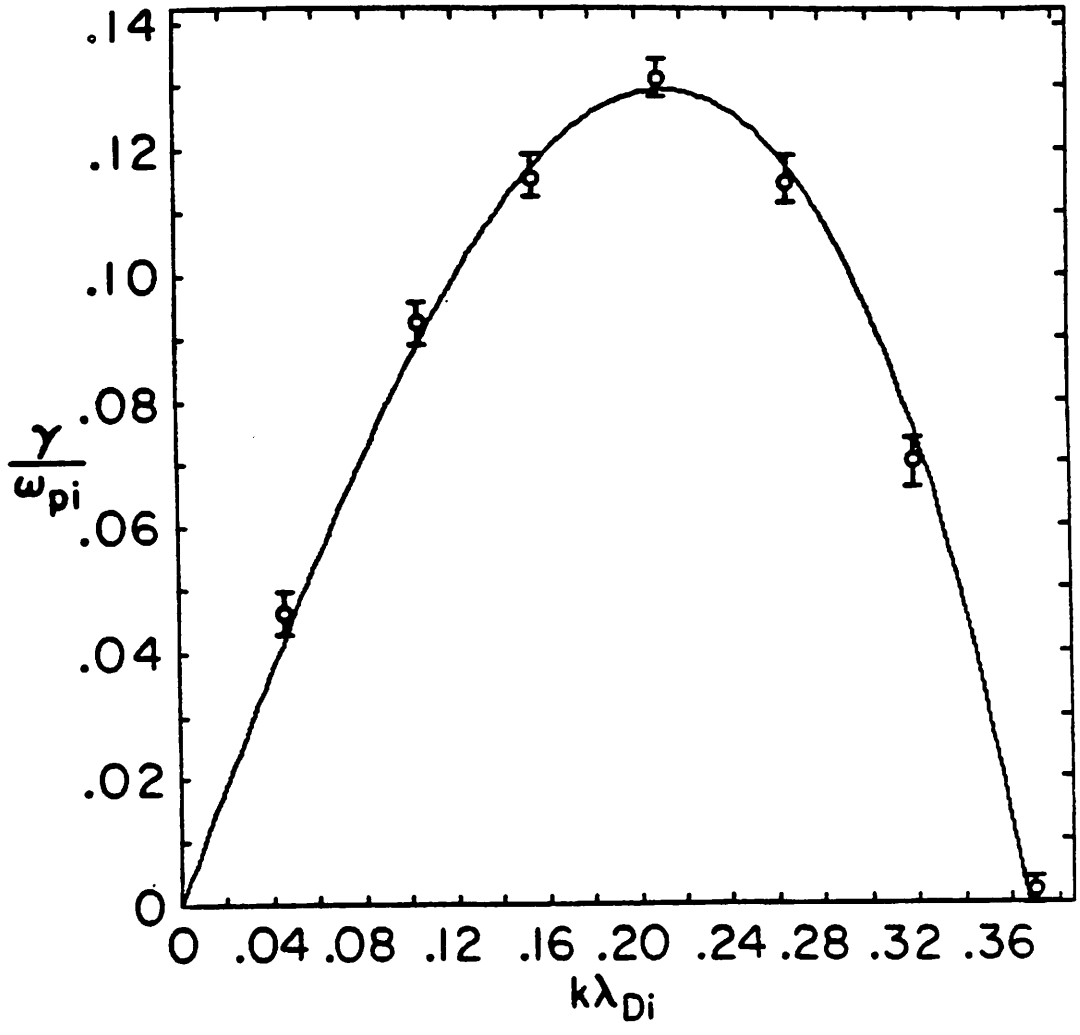

FIG. 8. Growth rate vs. $k\lambda_{Di}$ for $T_i/T_{e\,eff.} = 0.0635$, $\alpha = 1.9$, and $u = 2.0$. The circles represent simulation data from single mode simulations.

throat to the magnitude of the local axial magnetic field. The parameter T_i represents the central cell temperature and does not control the width of the ion distribution function.

In order to examine the instability for different growth rates the effective electron temperature was changed. Changing the effective electron temperature changes the maximum growth rate for the instability and it also changes the wavelength corresponding to the most unstable mode. The particle simulations make it possible to determine the nonlinear saturation level for the perturbed field. These simulation results are then used to generate a scaling law in terms of the growth rate.

The simulations were performed with the parameters $NG = 512$, $\omega_{pi}\Delta t = 0.2$, $n_{th}/n_{ECRH} = 0.5$, $L/\lambda_{Di} = 400$ and $NP = 70{,}000$. Here NG is the number of grids and NP is the number of particle ions. Only about a dozen modes were kept in the system. The large number of particles was essential to verify linear growth rates for very slowly growing modes. Also the saturation levels for the weakly unstable modes were very low which demands the least noise possible. The ions were initially loaded with a ordering scheme designed to fill phase space uniformly while at the same time avoiding unphysical beaming instabilities as explained in Ref. 15. This type of " quiet start " was necessary to examine cases with γ/ω_{pi} less than about 0.02. Cases with larger growth rate could be examined with a completely random start. We note that these simulations would have been virtually impossible using particle electrons because of the extra noise that would be created by them and because of the time step constraint imposed by the high frequency electron oscillations.

4.B: Simulation Results

A typical simulation had γ_{max}/ω_{pi} on the order of 0.05 with $k\lambda_{Di} = 0.10$. Contour plots of γ_{max} and the corresponding wavelength for the simulation parameters are shown in Fig. 8. The ratio of the effective electron temperature to the ion temperature was varied from its value at marginal stability to one hundred to one. At least two orders of magnitude of growth were observed in the field energy of the most unstable mode. The growth rates agreed well with theory. The purely growing characteristic of the instability was sometimes obscured by the

existence of other stable modes in the system for those cases where the maximum growth rate was small, that is γ_{max}/ω_{pi} smaller than 0.03.

After a linear stage of growth the growth rate decreases as the particles began to become trapped by the wave. At a later time the field energy reaches a peak and starts to decay. The phase space for this saturated stage of the wave is shown in Fig. 9 where the particle trapping is evident.

The final shape of the function $f_i(v_z)$ is an important quantity. In Fig. 10 this function is shown for four of the simulations. The gradual change in the appearance of the distribution function at saturation can be seen. Associated with this change is an increase in the value of the perturbed potential at saturation. In particular we see that at the higher saturation level the number of ions in the trapped region of phase space has increased substantially.

By examining many sets of simulations we find that the ion parallel distribution function in the saturated state remains double peaked to some extent until the linear growth rate is about $0.15\omega_{pi}$. So for linear growth rates lower than that value the saturation is in some sense a " soft " relaxation in that all of the free energy is not removed. However in general, $f_i(v_z)$ fills in more than required to satisfy marginal stability even when it remains bimodal. For example, the distribution function in Fig. 10 (a) is close to marginal stability while the distribution function in Fig. 10 (d) is clearly beyond marginal stability (i.e. more stable).

One diagnostic of particular relevance to the thermal-barrier problem is the quantity $\left(e\delta\phi/T_i\right)_{sat.}$, the value of the perturbed potential at saturation. In Fig. 11 this quantity is shown for the different ratios of the effective electron to ion temperature. The magnitude of the perturbed potential at saturation is important since if the instability leads to only a small value for the perturbed potential then one should expect that the thermal-barrier would be only slightly affected. On the other hand a large perturbed potential could cause a drastic change in the particle distribution function and hinder the operation of the thermal-barrier cell. This is consistent with Fig. 10. We note that for a significant amount of parameter space near marginal stability the saturated potential is small.

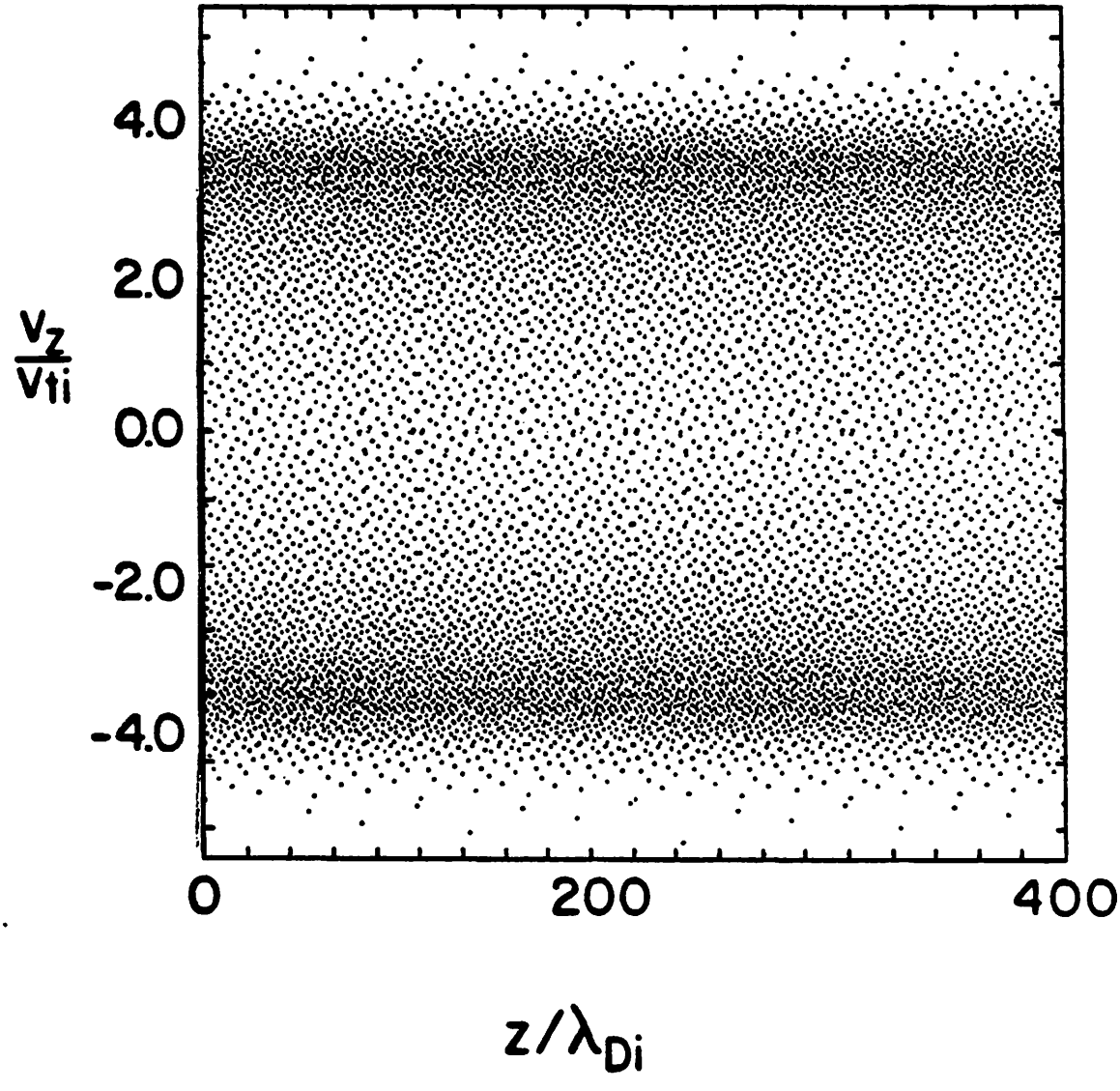

FIG. 9. Ion phase space for $T_i/T_{e\ eff.} = 0.023$ at (a) $t = 0$ and (b) saturation of the field energy. The ordered initial conditions are evident in (a).

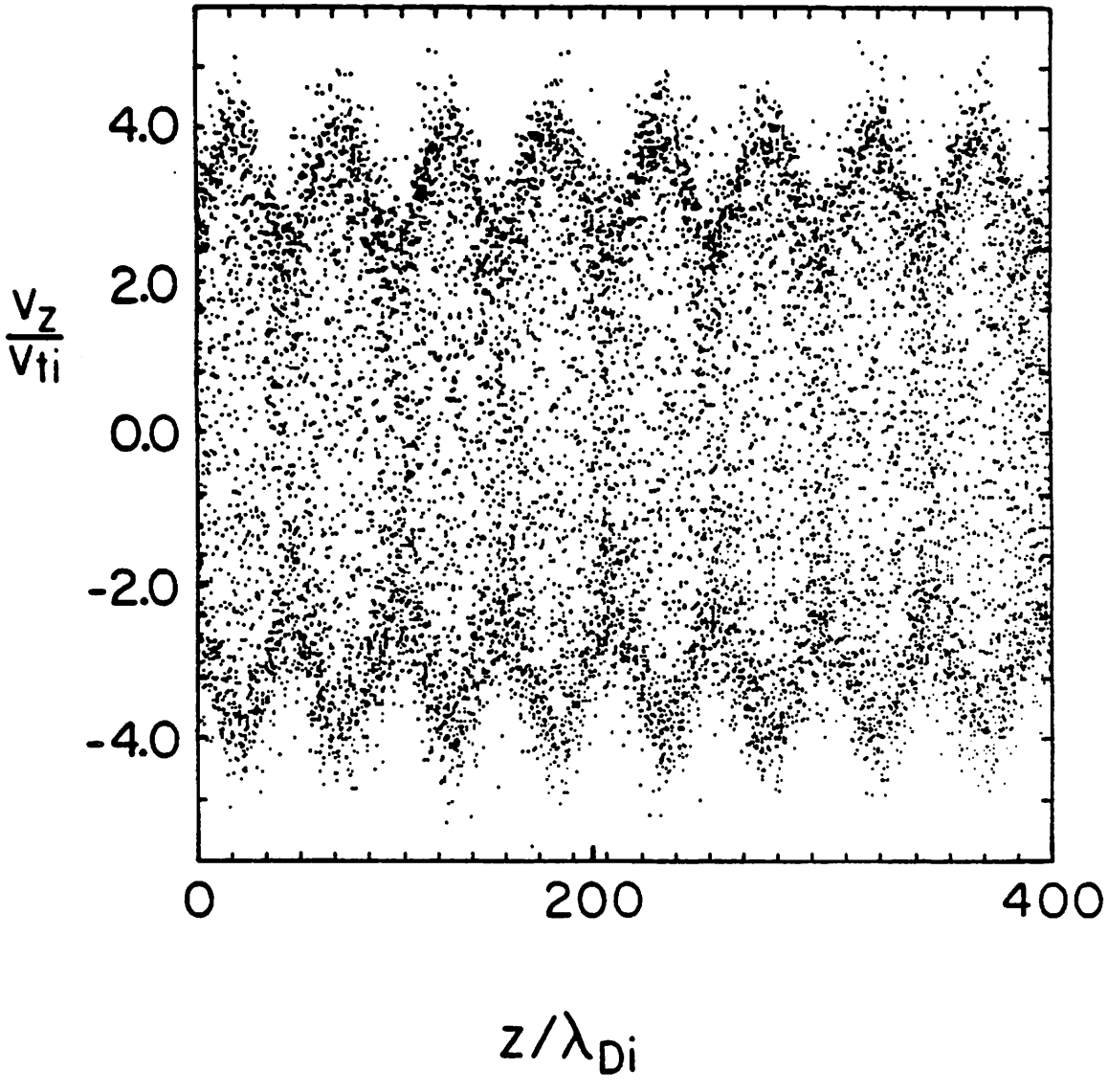

FIG. 9b.

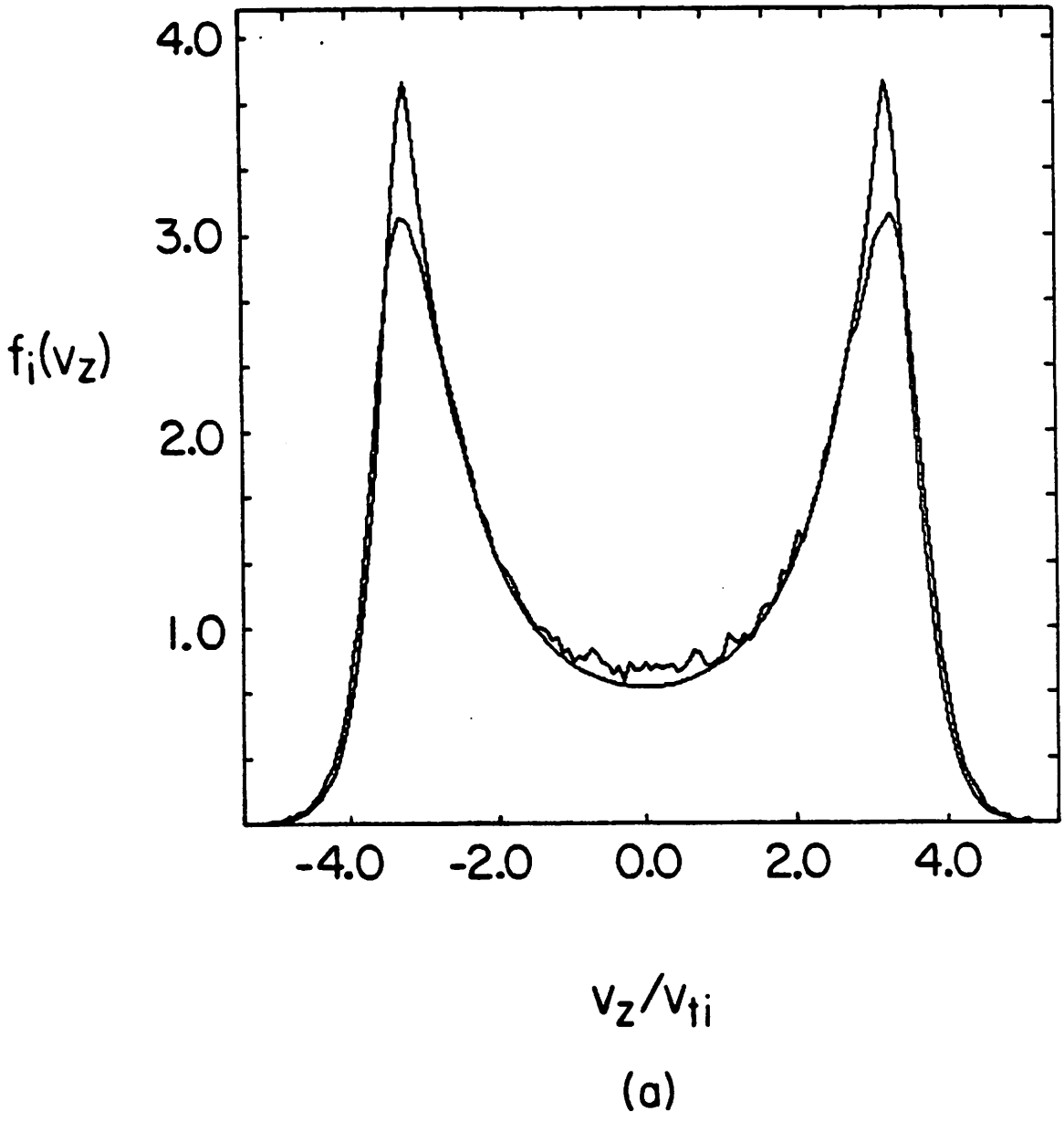

FIG. 10. Initial and final ion distribution function $f_i(v_z)$ (a) $T_i/T_{e\ eff.} = 0.054$, (b) $T_i/T_{e\ eff.} = 0.049$, (c) $T_i/T_{e\ eff.} = 0.043$, and (d) $T_i/T_{e\ eff.} = 0.023$.

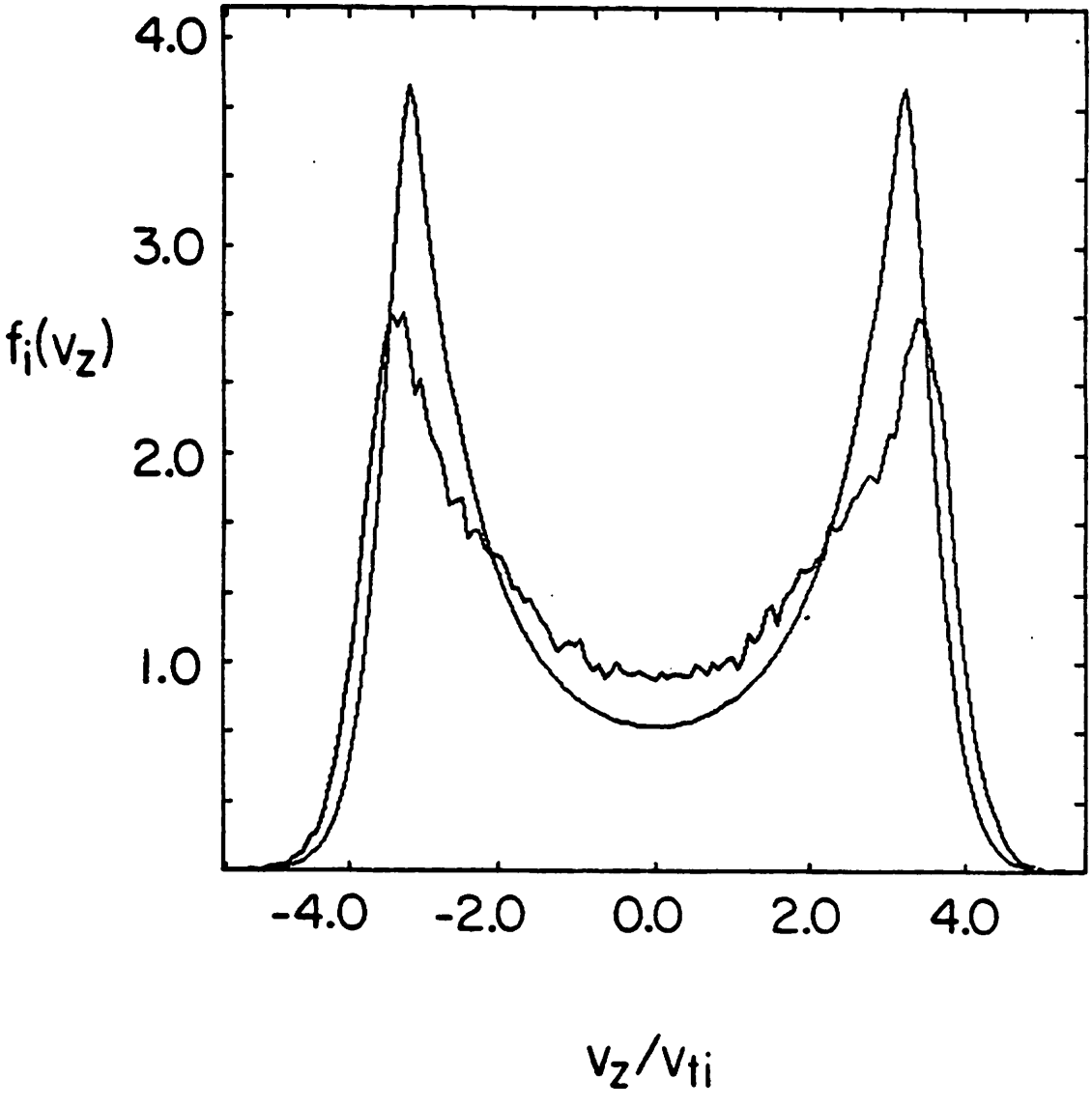

FIG. 10b.

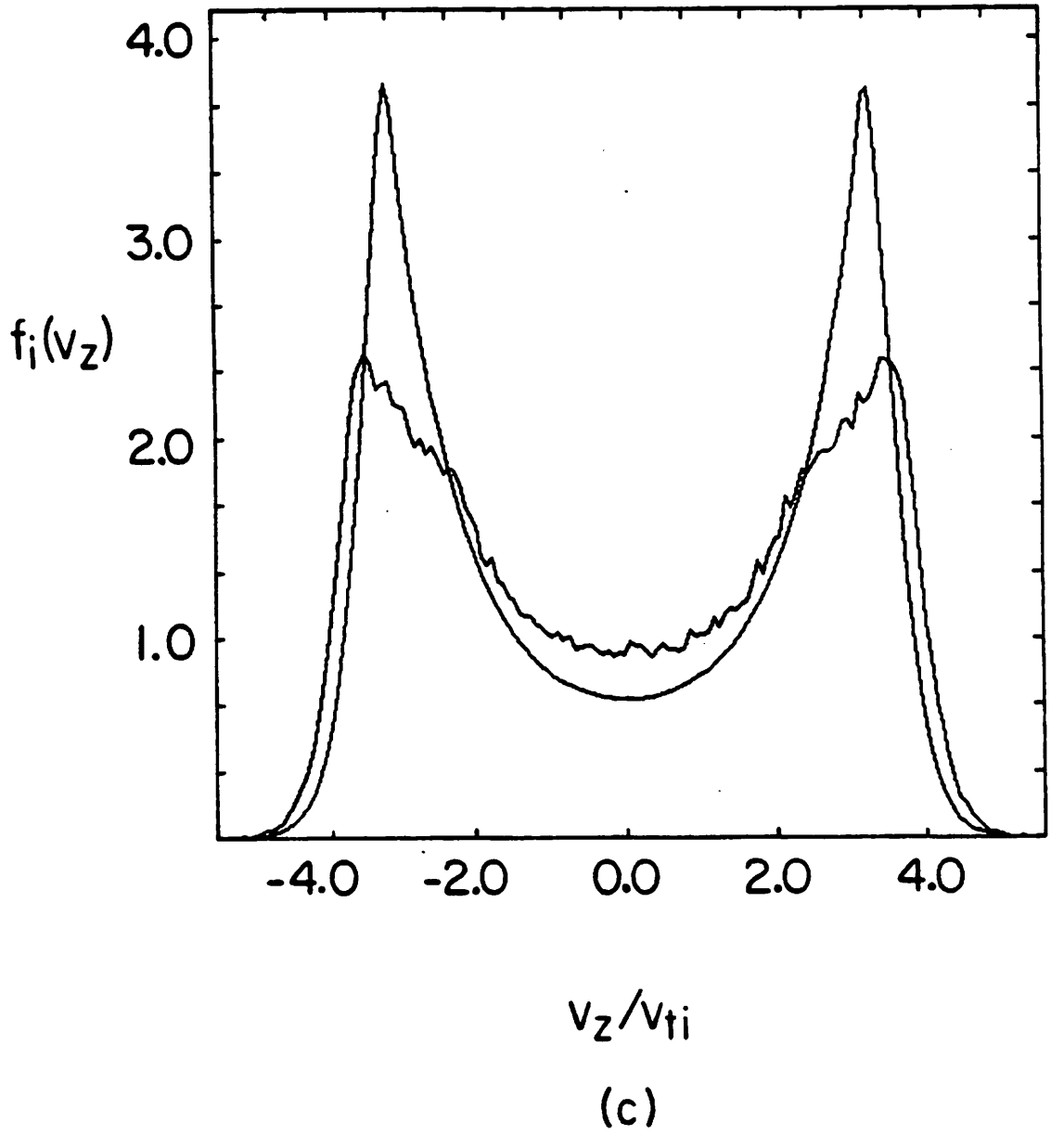

FIG. 10c.

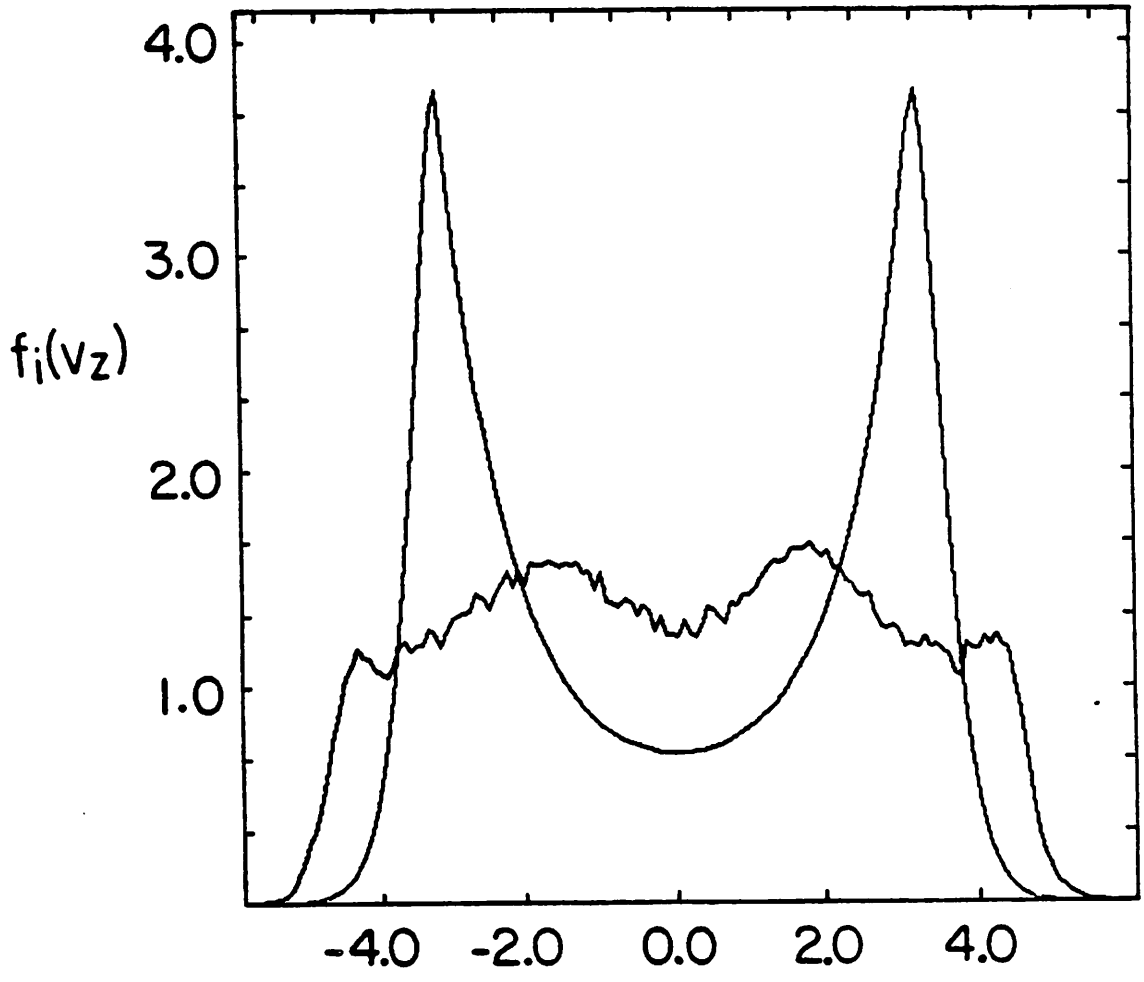

FIG. 10d.

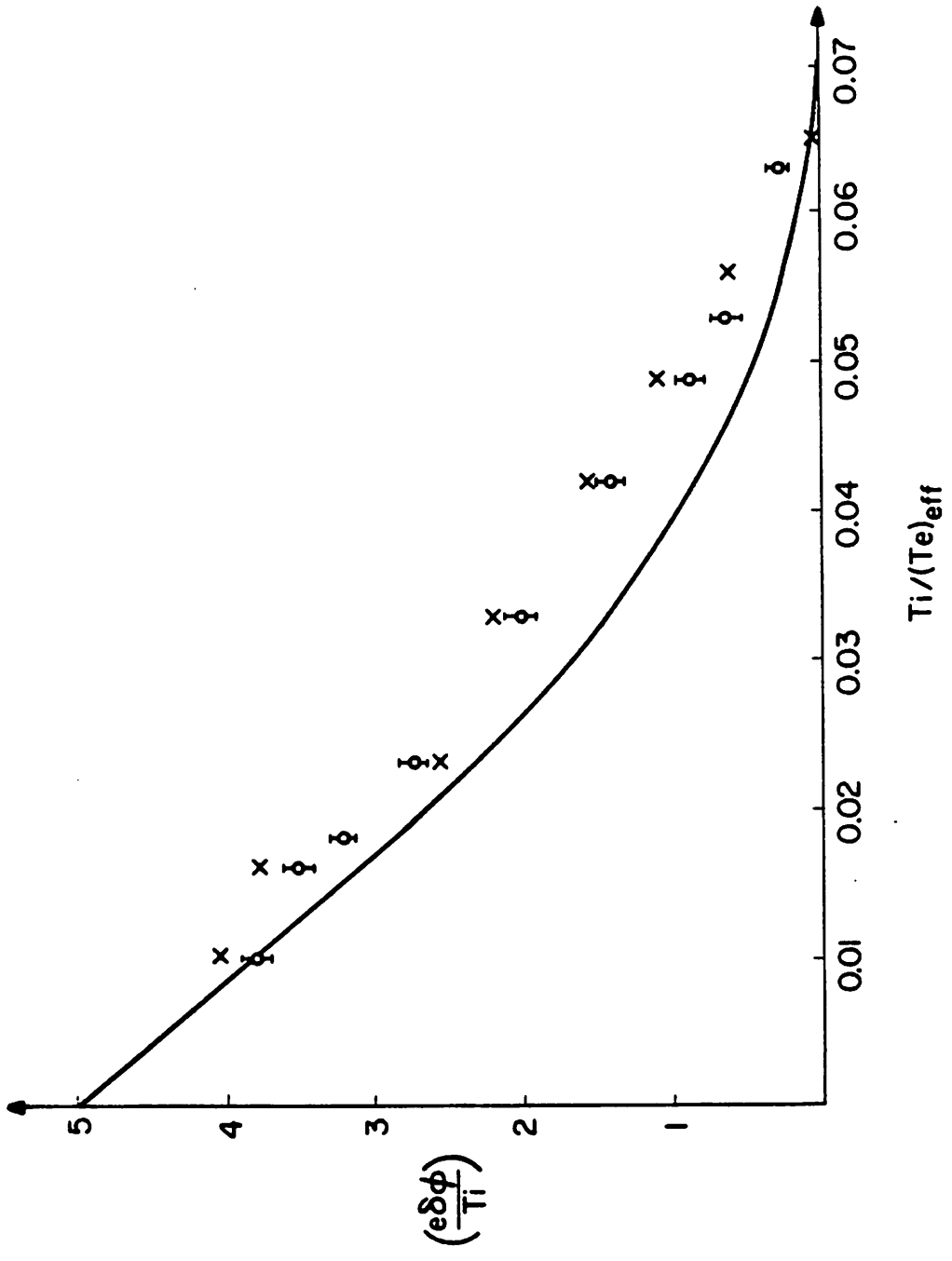

FIG. 11. Perturbed potential at the saturation of the field energy. The length of this system is $400\lambda_{Di}$ where λ_{Di} is the Debye length of the passing (thermal) ions. The crosses represent simulations retaining only the most unstable mode present in the system. The amplitude of the perturbed potential is easily determined from the simulation for this case. The dots on the other hand represent the simulations which retained many modes. The amplitude of the resulting perturbation is not exactly defined in this case. The value given in the figure represents an attempt to define an " average " amplitude from the simulation output. The line is from the estimate presented in the text.

The solid line in Fig. 11 represents an estimate for the maximum potential at saturation, obtained from an heuristic approach. We attempt to generate a scaling law for the perturbed field amplitude at saturation by assuming that saturation will occur in about an e-folding time of when the system becomes nonlinear. Linear theory breaks down when ω_{tr} is comparable to γ where ω_{tr} is the trapping frequency and γ is the linear growth rate of the unstable mode . Estimation of the perturbed field level at saturation by this technique yields a scaling law consistent with the simulations as shown in Fig. 11.

This estimate may be more precisely defined. If the instability is strong enough, the particle potential energy in the wave would be comparable to its initial drift energy. This gives $\frac{1}{2}m\ v_{\max}^2 = \left(e\delta\phi\right)_{sat}$ where $v_{\max}$ is the position of the peak in $f_i(v_z)$. This can be rewritten to read $\left(e\delta\phi/T_i\right)_{sat} = 0.5\left(v_{\max}^2/v_{ti}^2\right)$. This approximation as it stands is not yet sufficient to generate the desired scaling law because it predicts the same saturation level regardless of $T_{e\ eff.}/T_i$, i.e. , even when the distribution is stable. However , as argued in the preceeding paragraph the perturbed potential amplitude is proportional to the quantity $H = \gamma^2/(k\lambda_{Di})^2$. So multiplying our simple estimate by the ratio of the H quantities for finite electron temperature and infinite electron temperature gives the desired expression. This is the quantity that is given in Fig. 11. Note that a better fit to the simulation data could have been obtained by treating the scale function as a free parameter.

The field energy in the unstable modes increases monotonically from approximately 2×10^{-5} to 2×10^{-2} of the initial ion kinetic energy as the ratio of the effective electron temperature of the ion temperature is changed from 0.065 to 0.01. The quiet start field energy was approximately 5×10^{-7} of the ion kinetic energy.

The period after saturation, when the total field energy decreases is important also. The particle phase space vortices due to the trapped particles begin to coalesce, and the bulk of the field energy is deposited into longer wavelengths. The maximum peak-to-peak potentials do remain roughly constant at least during the initial phase of the post saturation process. Later on, as the ion phase space vortices coalesce the peak potentials may in fact become larger than

the corresponding magnitudes at saturation of the field energy. Large amplitude residual fluctuations on the order of $e\delta\phi/T_i = 1$ persist for times on the order hundreds ion plasma periods.

We must mention, however, that the details of the post saturation period are open to question since during this time the particles have managed to cross the entire periodic system. Also finite length effects should come into play in a real system as the dominant wavelength becomes larger and larger. In addition, the existence of plasma flux from the boundaries has not been included. The most serious omission is that the potential of the simulation region relative to the central cell has not be updated (In fact it is not possible to update this potential of the simulation region relative to the central cell in a self consistent manner using this simple uniform model). This is why we have chosen our simulation parameters so that $e\delta\phi/T_e$ always remains much smaller than unity. Some of these objections concerning the boundary conditions and finite length effects are eliminated by the nonuniform simulations presented in the next section.

5. The Ion-Ion Two-Stream Instability in the Inhomogeneous Limit

This section consists of two parts. The first part deals with some modifications to the theory for the ion-ion two-stream mode caused by axial inhomogeneities. The second part deals with our particle simulations in this axially nonuniform limit.

5. A: Theory

As shown in Section 3. the electrostatic ion-ion two-stream mode has characteristic wavelengths of on the order of $50\lambda_{Di}$ for parameters of interest in thermal-barrier cells. These wavelengths are much shorter than the length of the thermal-barrier cell, but may or may not be shorter than the relevant region of instability. Therefore we now consider a WKB approach to determining the linear behavior un this nonuniform medium; i.e. the solution is chosen to have the form $\delta\phi(z) = \psi(z)e^{ik_0 z}$ where $\psi(z)$ contains the slow variation in the mode structure.

We start by expanding the dispersion relation $D(\omega,k;parameters)$about the potential minimum in the thermal-barrier cell. We also take advantage of the fact that the dielectric

function is a real function for real k and imaginary ω . This simplifies the analysis considerably. Limiting our attention to real k and imaginary ω is valid if tunneling of the mode to other regions can be ignored. For our problem this is justified since the mode is confined to a small region near the cell minimum. Our expansion yields

$$\frac{\partial D}{\partial \gamma}\delta\gamma + \frac{\partial^2 D}{\partial z^2}(\delta z)^2 + \frac{\partial^2 D}{\partial k^2}(\delta k)^2 = 0. \tag{7}$$

Here all of the partial derivatives are evaluated at $z = z_0, k = k_0$ and $\gamma = \gamma_0$ with z_0 being the position of the barrier minimum, and k_0 and γ_0 corresponding to the most unstable mode (according to local analysis) at the cell minimum. We have also made use of the relations $D_z = 0$, $D_k = 0$, and $D(z_0,k_0,\gamma_0) = 0$. There are no cross terms of the form $(\delta k)(\delta z)$ since $D_z = 0$ at the cell minimum for all k and γ.

Transforming back from Fourier space gives the Weber-Hermite equation for the function $\psi(z)$ with eigenvalues

$$\delta\gamma = \frac{(D_{zz}D_{kk})^{1/2}}{-D_\gamma}\,(N + \frac{1}{2}) \tag{8}$$

with N a nonnegative integer. The eigenfunctions are the usual harmonic oscillator solutions

$$\psi_N(z) = H_N(y)\,\exp\left[-\frac{y^2}{2}\right] \tag{9}$$

where $y = (z - z_0)/(\Delta z)$ with

$$\Delta z \equiv \left[\frac{D_{kk}}{D_{zz}}\right]^{1/4} \tag{11}$$

and H_N is the usual Hermite polynomial of order N . The complete mode structure $\delta\phi(z)$ is then obtained by multiplying the function $\psi(z)$ by the function $e^{ik_0 z}$. For this specific problem it is possible to show in general that D_{zz} , D_γ, and D_{kk} are all positive. This means finite length effects are stabilizing and the mode remains purely growing.

The solution $\psi(z)$ corresponding to $N = 0$ is the most unstable mode. For the equilibria that have been constructed it appears that the quantity $(\delta\gamma)/\gamma$ remains less than 0.1 as long as there are more than about two wavelengths in a region of width $2\Delta z$. For smaller numbers of wavelengths in a interval of that width our original expansion breaks down complelety and a

correct analysis would have to include higher order terms in both z and k. In any event, the simulation results give qualitatively similar behavior.

5. B: Particle Simulations

Here we present some results for axially nonuniform simulations. Important quantities to examine include the magnitude and spatial distribution of $e\delta\phi/T_i$ at saturation, the final appearance of the distribution function $f_i(v_z)$, the ion density, $n_i(z)$, and any effects due to inhomogeneity such as the mode structure of the unstable modes.

The equilibrium for these simulations was constructed by specifying $\phi(z)$, $B(z)$, and the ratio of the central cell ion temperature to the central cell electron temperature T_i/T_e; the quasineutrality condition then determines $n_{ECRH}(B)$. The functions $\phi(z)$ and $B(z)$ were required to be symmetric about the middle of the thermal-barrier cell. In addition, it was required that $\phi = 0$ and $d\phi(z)/dz = 0$ at the boundaries. The parameter $\alpha = 4.0$ and the potential of the center of the thermal-barrier relative to the central cell was taken to be $e\phi_{max}/T_i = -5.0$. The equilibrium axial potential and the ion density are given in Fig. 12.

Typical simulation parameters were $NG = 1024$, $NP = 100{,}000$, $\omega_{pi}\Delta t = 0.3$ (where ω_{pi} is calculated at the maximum ion density), and the system length was a parameter to be varied. As before, NG represents the number of grids and NP represents the number of particles. The ions are treated as fully nonlinear particles; standard linear weighting is used. The ion density was fourier smoothed before the field solve; only linearly unstable modes were retained. Retaining shorter wavelengths only increased the noise level of the simulations. The effect of the axially varying magnetic field was modeled by adding a $\mu\nabla B$ force to the equations of motion and by weighting the particles proportionally to the local value of B (to account for the expansion of magnetic flux tubes). The incoming ion flux was held fixed at both boundaries as was the Maxwellian distribution function of these incoming ions. The electrons consisted of an energetic component $n_{ECRH}(B)$ and a Boltzmann response representing the central cell electrons. The several field solves are discussed in Appendix B.

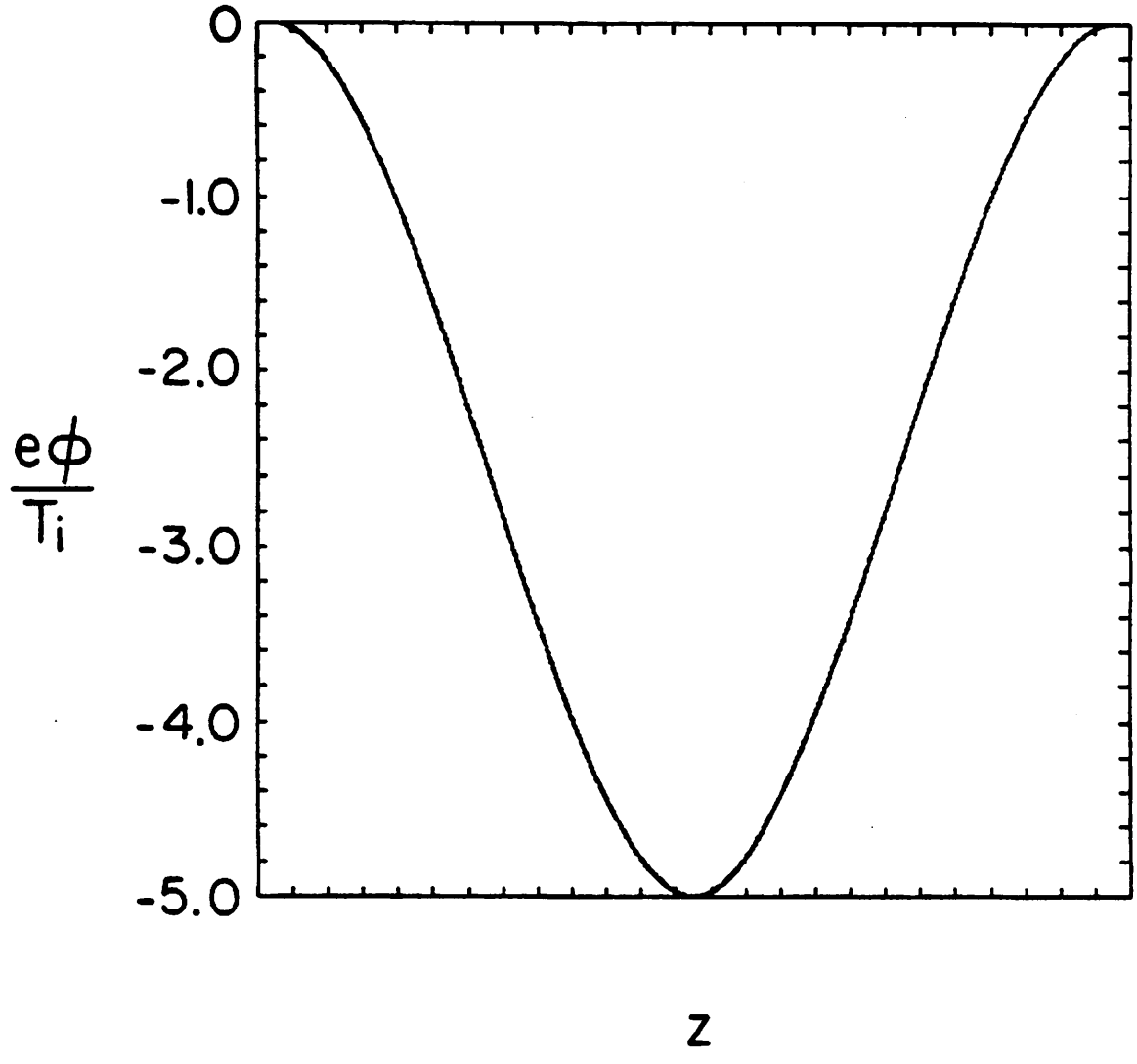

FIG. 12. Equilibrium (a) potential and (b) ion density for the axially nonuniform simulations. For this case the magnetic field profile is as in Fig. 2.

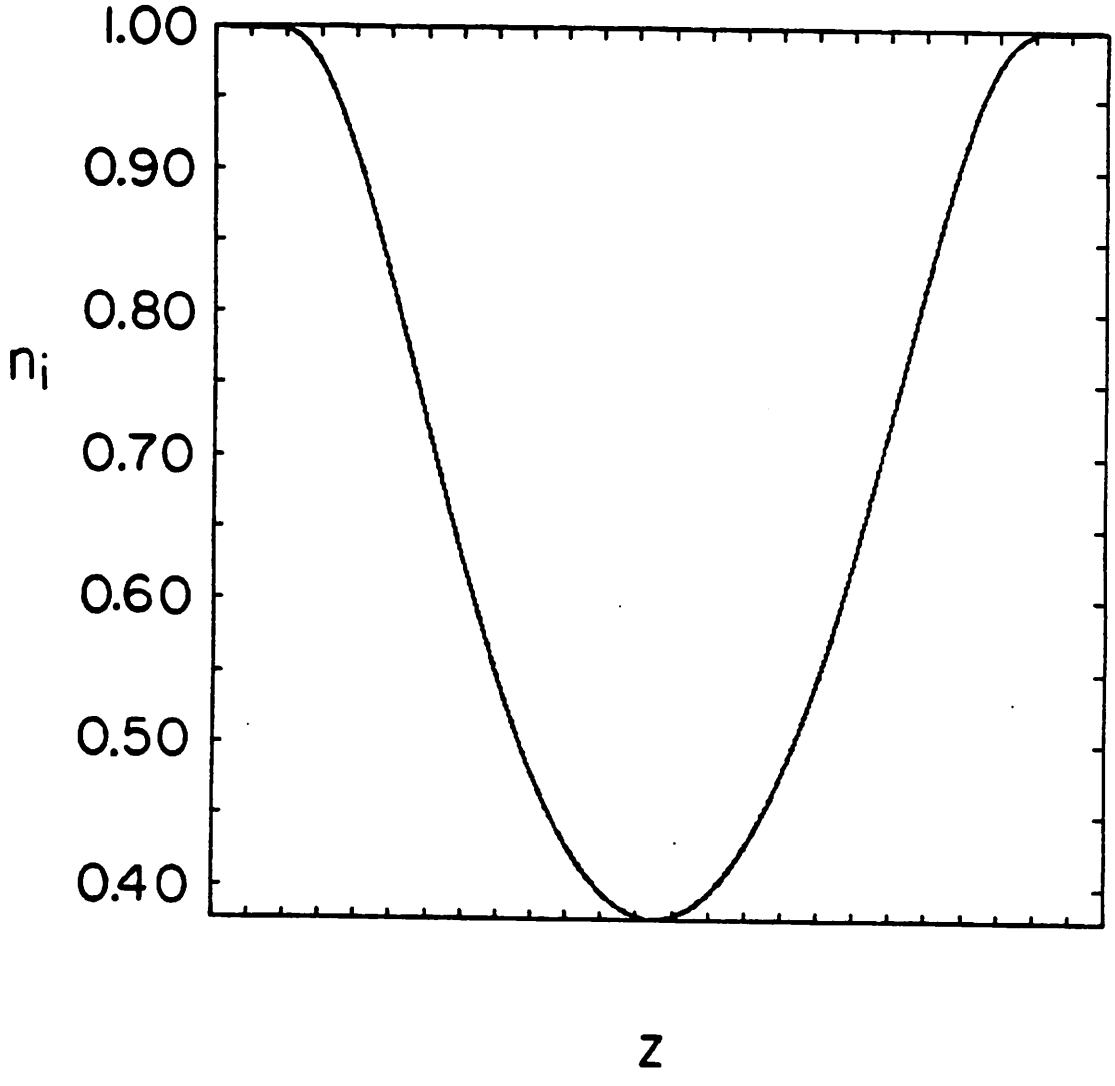

FIG. 12b.

In order to more properly examine the mode structure we performed a series of simulations in which the effective electron temperature was held fixed at the initial (equilibrium) profile. This eliminates nonlinear electron effects from the mode structure. The equilibrium used is as described above with $T_e/T_i = 1.0$. At the center of the thermal-barrier $T_{e\ eff.}/T_i = 0.017$ which corresponds to a very unstable equilibrium. Figure 13 shows examples of the mode structure and the effects of varying the system length. We note that it is difficult to make a direct comparison of these mode structures and the theoretical structure of the previous section since either (1) the unstable region is large compared to the most unstable wavelength in which cases many normal modes are present with similar growth rates or (2) the unstable region is not long compared to the most unstable wavelength in which case the finite length stabilization is very strong and the WKB analysis breaks down. In any event analysis of the mode structure does reveal the most unstable wavelength from uniform homogeneous theory in those cases where condition (1) is satisfied and shows that finite length effects are strongly stabilizing under condition (2).

It is instructive to compare the maximum deviation from the equilibrium potential ,$\Delta\phi_{max}$, in the nonuniform system (Fig. 13) with the mode amplitudes at saturation in the uniform system (Fig. 11). Note that, to the accuracy of the simulations, the values for $\Delta\phi_{max}$ are similar except under the most severve shortening of the unstable region ($\lambda \leqslant L$).

Inclusion of the fully nonlinear electron response is important to model the problem correctly. The nonlinear electron response allows a self-consistent filling in of the thermal barrier with central cell electrons. This will then determine the potential everywhere in a self-consistent manner. Results are presented below from a typical simulation.

For this simulation $T_e/T_i = 1.3$ which corresponds to $T_{e\ eff.}/T_i = 0.042$ at the center of the thermal-barrier cell. The length of this system is $1600\lambda_{Di}$, which may correspond to the appropriate physical dimension of some devices. Alternatively, the simulation region may be thought of as the unstable portion of a much longer system.

After a short period of time a mode structure appeared which had the wavelength

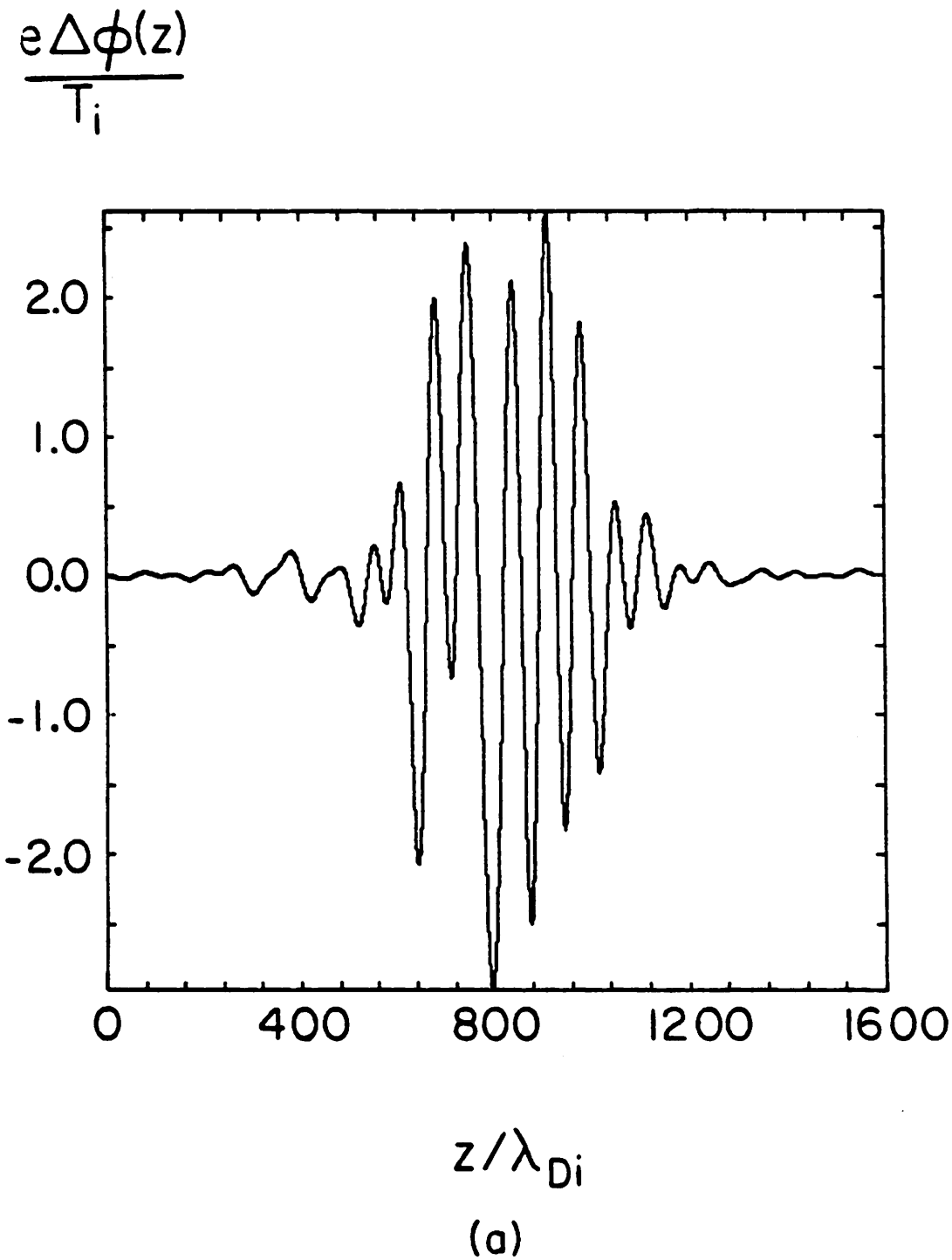

FIG. 13. The quantity $(e\Delta\phi(z))/T_i$ at saturation for (a) $L = 1600\lambda_{Di}$, (b) $L = 800\lambda_{Di}$, and (c) $L = 400\lambda_{Di}$. The quantity $\Delta\phi$ represents the difference between ϕ and the equilibrium value for ϕ. The ratio $T_{e\,eff.}/T_i = 0.017$ at the center of the cell.

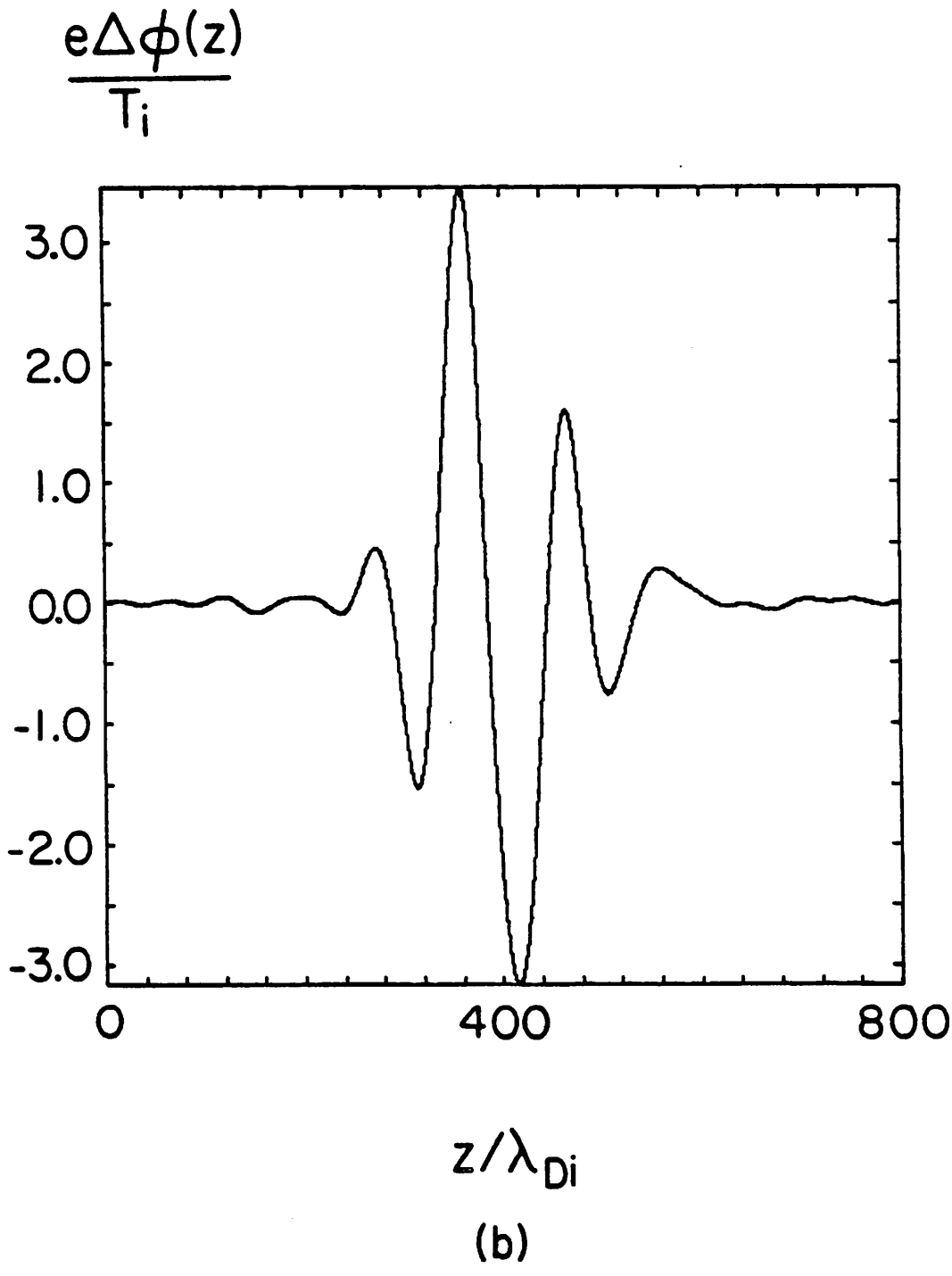

FIG. 13b.

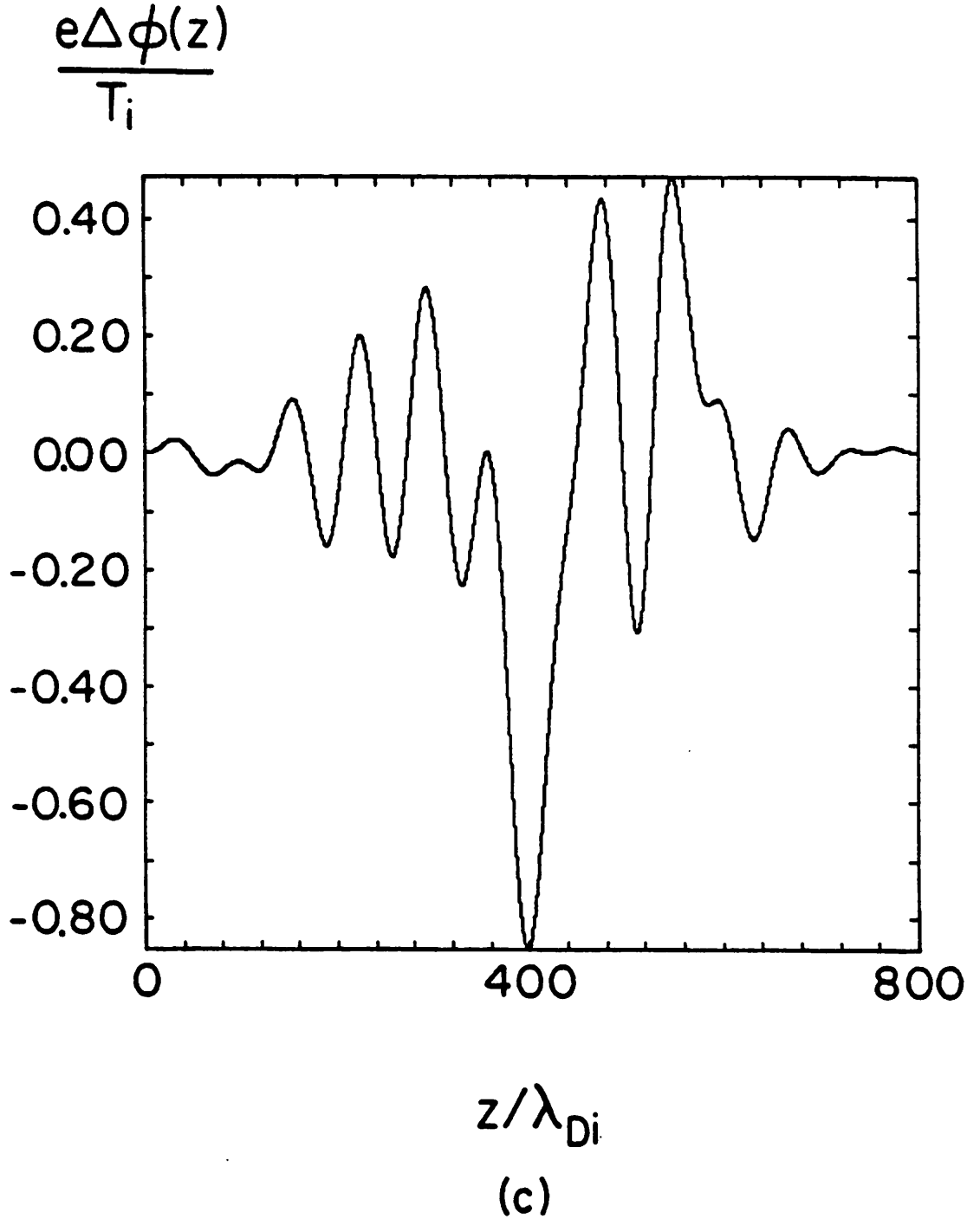

FIG. 13c.

corresponding to uniform homogeneous theory. As the amplitude grows the electrons become nonlinear as $e\delta\phi/T_e$ becomes of the order of and larger than unity. This manifests itself in the potential structure, with a waveform that has larger negative pertubations than positive perturbations. This is due to the assumed Boltzmann electron response. The Boltzmann approximation is valid as long as $\nu/\gamma \geq (e\delta\phi/T_e)$ where ν is the electron collision frequency and$\delta\phi$ represents any (positive) potential change from the equilibrium value which may trap passing electrons. The passing electrons are kept at a fixed temperature by the central cell.

As the ions become trapped the barrier is filled in to a certain extent. The central cell electrons also have an increase in density in the cell as they attempt to preserve quasineutrality. Figure 14. shows the ion density , Fig. 15 shows $\phi(z)$, and Fig. 16 gives $f_i(v_z)$ at the center of the cell long after the instability has saturated. Note that because the potential well has been filled in to a certain extent, the peaks in the ion distribution function occur at a smaller value of v_z. Also there are no longer fast ion tails as for the periodic cases presented earlier. This is due to the proper particle boundary conditions.

One feature charateristic of the post saturation period is the existence of large negative potential structures as in Fig. 15. These structures depend somewhat on the details of the simulation equilibrium. However, these structures are formed for all simulations except those very close to stability, and these structures persist for more than $1000\omega_{pi}^{-1}$. Including residual shielding from the energetic electrons (as discussed in Appendix B.) reduces the amplitudes of the structures but does not cause them to disappear.

From other simulations we conclude that the resulting filling in of the ion parallel velocity distribution $f_i(v_z)$ and the potential $\phi(z)$ are independent of the system length as long as there are more than about two or three wavelengths of the most unstable mode in the unstable region. This is consistent with the mode structure simulations.

It would be incorrect to claim that this instability has saturated only to marginal stability, however. There are two independent reasons for this. First, finite values for the growth rate cause some amount of overshoot in the filling in of ion phase space as in the periodic

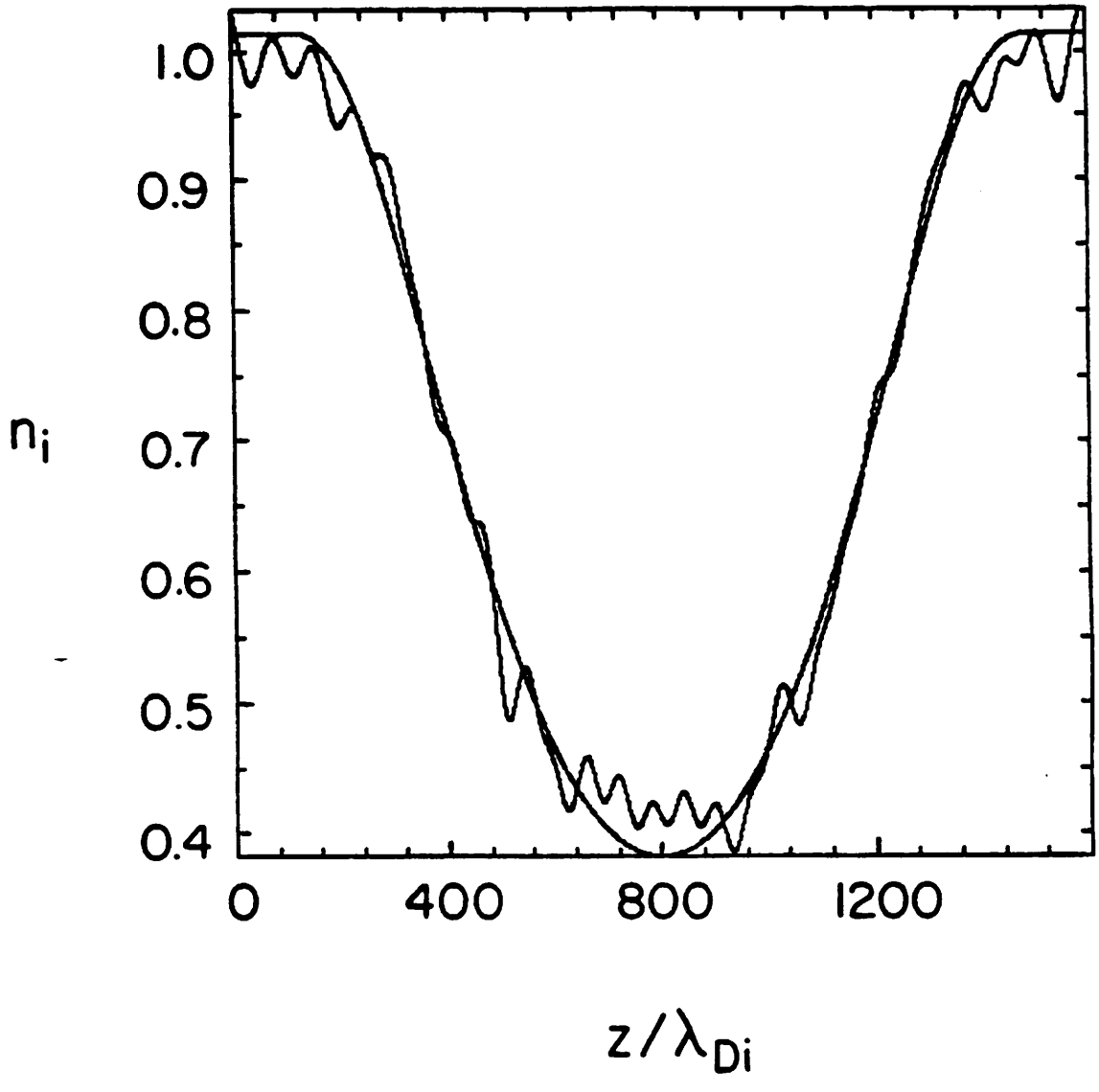

FIG. 14. Ion density at $t = 500\omega_{pi}^{-1}$ (roughly one half of the transit time across the system for a typical ion) . The smooth curve represents the equilibrium value. Note that the ion density at the cell center has increased by only about fifteen percent. Also note the density depressions at the edges due to some of the passing ions being captured in the well.

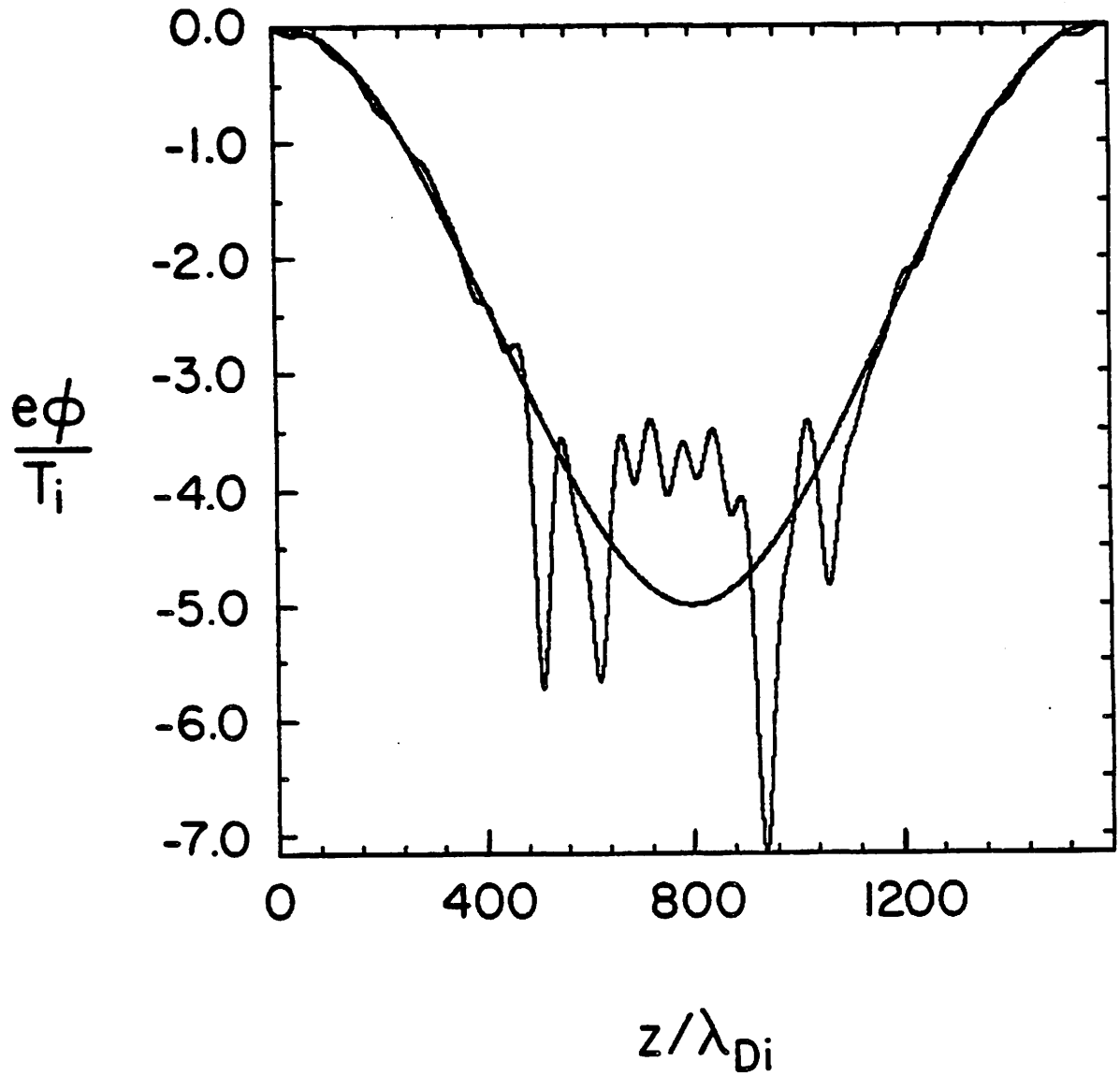

FIG. 15. The quantity $(e\phi(z))/T_i$ at $t = 500\omega_{pi}^{-1}$. The smooth curve represents the equilibrium potential.

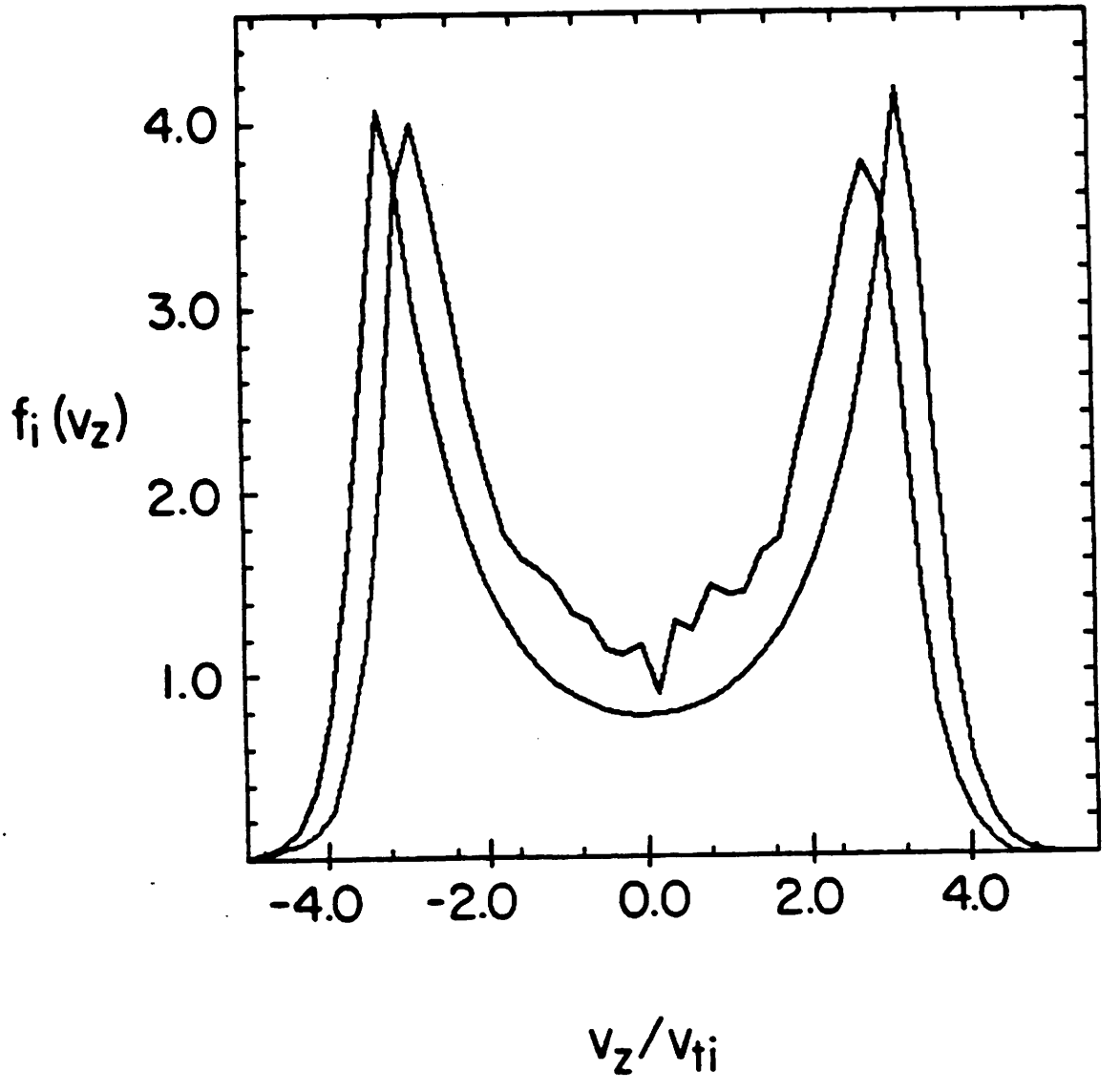

FIG. 16. Ion distribution function at the center of the cell at $t = 500\omega_{pi}^{-1}$. An average has been taken over one tenth of the system length. The smooth curve represents the distribution function at $t = 0$.

simulations. Secondly, the density of central cell electrons in the thermal-barrier cell also increases in order to maintain quasineutrality. This in turn causes the stabilizing electron shielding to increase which causes a decrease in the well depth. This then causes the ion streaming velocity to be lower in the center of the thermal barrier cell.

The last consideration may be especially important for negative tandem mirrors. For a negative mirror the thermal electron density at the center of the thermal-barrier is virtually zero. An instability causing an increase in the ion density may cause a equal increase in the thermal electron density, since the energetic electrons will not respond to the electric fields. To obtain that increase in the thermal electron density the potential may have to be increased substantially.

In this regard the collisionless trapping of the thermal electrons becomes very important since the electrons would not be able to come to thermal equilibrium on the time scale of the instability. As shown in Ref 16. the trapped electron density increases no faster than $\left(e\delta\phi/T_e \right)^{1/2}$ under very general conditions where $\delta\phi$ is the depth of the trapping potential i.e., much slower than the Boltzmann response would predict. Using this type of electron response implies that the potential peaks could be much larger that one obtains from using the Boltzmann response.

The simulation presented in this section is indicative of the behavior of the instability close to marginal stability and collisional enough so that the Boltzmann approximation is valid. The other limit of compleletly collisionless electrons will be presented in a future publication.

6. Conclusions and Concluding Remarks

In this paper we have presented thermal-barrier equilibrium studies using two different models for the ion population. In our analysis, we have examined how the various equilibrium parameters impact on the stability of the field aligned electrostatic ion-ion two-stream modes. We have found that stability is certainly model dependent and that unstable parameter regimes do exist, but it appears that for parameters of greatest interest (i.e., applicable to TMX-U and MFTF-B), the thermal-barrier equilibria are stable.

Simulations in 1-d have been done, both in a spatially uniform periodic system and in an axially nonuniform system, and have given some insights into the nonlinear consequences of this instability. For fairly large regions of parameter space, the instability saturates with only a slight increase of the number of ions in the trapped region of the ion phase space. The instability thus causes only small changes in the depth of the thermal-barrier potential well and should prove innocuous to the barrier.

Finite-length effects are such as to decrease growth rates, however this stabilization is insignificant when $L >> \lambda$. Here L is the length of the unstable region and λ is the wavelength of an unstable mode. Fluctuations are strongly stabilized by finite length effects when λ is comparable to the length of the unstable region.

The authors appreciate useful discussions with Professor C. K. Birdsall, Dr. J. A. Byers, Dr. B. I. Cohen and Dr. T. L. Crystal.

This research was partially supported by the Office of Naval Research Contract No. N00014-77-c-0678 (Berkeley), and in part by the Department of Energy under Contract No. DE-AM03-76SF00034 (Berkeley). The computations were performed at the National Magnetic Fusion Energy Computer Center at Lawrence Livermore National Laboratory.

Appendix A.

Here we discuss the model ion distribution function of Cummins[10]. His model was developed to model the same Folkker-Planck simulation results as that of Ref. 7. However, the agreement between the model and the simulation results are better for the model of Ref. 10. Our interest in the distribution function is to try and gain understanding of to what degree our equilibrium problem is model dependent.

The distribution function is most easily expressed in prolate spherical coordinates;

$$\begin{aligned} v_x &= \Theta \sinh(u)\, \sin(\psi)\, \cos(\chi) \\ v_y &= \Theta \sinh(u)\, \sin(\psi)\, \sin(\chi) \\ v_z &= \Theta \cosh(u)\, \cos(\psi) \end{aligned} \tag{A1}$$

where $\Theta = ((R/(R-1))2e(-\phi)/m)^{1/2}$, R is the local mirror ratio, and ϕ is a potential

difference between the point in the thermal-barrier cell and the central cell. This model is good only for ϕ negative. The variables have the limits $0 \leqslant \psi \leqslant \pi$, $0 \leqslant \chi \leqslant 2\pi$, and $0 \leqslant u \leqslant \infty$. Using these variables the separatrix may be expressed as

$$\cos^2(\psi) = (R - 1)/R. \tag{A2}$$

Finally, the ion distribution can be represented as

$$f_{t,p} = n_0(m/2\pi T)^{3/2}\exp(a1)\exp(-a2(\sinh^2(u) + \cos^2(\psi) + g(\cos(\psi))) \tag{A3}$$

where $a1 = -e\phi/T$, $a2 = -a1(R/(R - 1))$, and $g(\cos(\psi))$ is any function of ψ that goes to zero on the separatrix. This will ensure that the distribution function is continuous at the separatrix, a condition which must be realized in any physical equilibrium.

For our calculation we have used

$$g(\cos(\psi)) = \eta\left(\frac{R-1}{R} - \cos^2(\psi)\right) \tag{A4}$$

with η a constant. The quantity ν in Fig. 7 represents $1/\eta^5$ in order to appear qualitatively the same as Fig. 6 for the parameters of most interest.

Appendix B.

In this appendix we discuss the field solve and the boundary conditions used in our particle simulation code. We follow the procedure in Mason[14] . Poisson's equation for our system reads

$$\nabla^2\phi = e(n_e - n_i) \tag{B1}$$

where n_i is a grid quantity collected from the particle ions and the electron density is given by

$$n_e(\phi,B) = n_0 e^{e\phi/T_e} + n_{ECRH}(B) \tag{B2}$$

and q is the charge of an ion. On the right hand side of (B2), the first term represents the warm thermal electrons and the second term represents the fixed charge density due to the energetic mirror trapped electrons. Rewriting Poisson's equation we obtain

$$\nabla^2\phi = e(n_0 e^{e\phi/T_e} - (n_i - n_{ECRH}(B))). \tag{B3}$$

Taking the derivative of this equation with respect to z gives

$$\nabla^2 E = -e(En_0(-e/T_e)e^{e\phi/T_e} - \nabla n_i^*) \tag{B4}$$

or rewritten

$$\nabla^2 E - e\nabla n_i^{\bullet} = (\nabla \cdot E - e n_i^{\bullet}) E(-e/T_e) \tag{B5}$$

where $n_i^{\bullet} = (n_i - n_{ECRH})$. This equation may be solved for in an iterative manner as in Ref. 14. Their boundary conditions were $E(0) = 0$ and $E(L) = 0$. For our simulations we use periodic boundary conditions to close the set of equations. We also require that the average electric field be zero. This condition may be written as $\int_0^L E dz = 0$. A correction at each iteration of

$$\mathbf{E}^j = \mathbf{E}^j - \mathbf{E}_{ave} \tag{B6}$$

is used before proceding with the $j + 1^{th}$ iteration. Here $\mathbf{E}^j$ is to be considered a vector of dimension NG and $\mathbf{E}_{ave}$ is the average electric field across the system.

The effective electron temperature profile may be kept constant in the following manner. Rewritting Eq. (B5) gives

$$\nabla^2 E - e\nabla n_i^{\bullet} = (\nabla E - e n_i) E(-e/T_e(z)) \tag{B7}$$

where $e/T_e(z) = n_e(\phi)/(dn_e(\phi)/d\phi)$. This $T_e(z)$ represents the effective electron response as a function of position. Keeping its value fixed at the equilibrium values allows one to concentrate on the ion behavior.

When the number of grids becomes very large (on the order of 1×10^3) and $e\delta\phi/T_e$ increases to and above unity there is another method which requires significantly fewer iterations[17,18] to solve Eq. (B1) with Eq. (B2). The procedure is to solve Eq. (B1) with Eq. (B2) given an initial, close guess for ϕ. This results in iteration of

$$\nabla^2 \phi_j{}^p = e \left[n_0 e^{e\phi_j{}^{p-1}/T_e} \left[1 + \frac{e(\phi_j{}^p - \phi_j{}^{p-1})}{T_e} \right] - n_i^{\bullet} \right] \tag{B8}$$

where $\phi_j{}^p$ is the p^{th} iteration for the potential at the j^{th} grid point. This technique was used for nonuniform simulations with the potential fixed at both boundaries. At each iteration a tridiagonal matrix equation must be solved. The results from this field solve are consistent with the results of the other nonlinear field solve. As explained in Ref. 18, this type of field solve is expected to show rapid convergence. The extention to multi-dimensional field solves is also

possibile. We note that it is also possible to linearize the electron response about the equilibrium with this field solve and we have done so. In addition it is straight foward to include shielding from the energetic electron component.

References

1. E. A. Foote and R. M. Kulsrud, Phys. Fluids **24** , 1532 (1981).
2. F. W. Perkins, Phys. Fluids **19** , 1012 (1976).
3. E. S. Weibel, Phys. Fluids **13** , 3003 (1970).
4. D. W. Forslund and C. R. Shonk, Phys. Rev. Lett. **25** , 281 (1970).
5. T. E. Stringer, Plasma Phys. **6** , 267 (1964).
6. M. Lontano, L. S. Pekker, and R. Pozzoli, Fiz. Plazmy **6** , 793 (1980). [Sov. J. Plasma Phys. **6** (4), 432 (1980)]
7. R. H. Cohen, Nuclear Fusion **21** ,289 (1981).
8. D. E. Baldwin and B. G. Logan, Phys. Rev. Lett. **43** , 1318 (1979).
9. I. B. Bernstein, J. M. Greene, and M. D. Kruskal, Phys. Rev. **108** ,546 (1957).
10. W. F. Cummins, private communication.
11. L. D. Pearlstein and W. M. Nevins, " The Barrier Potential Model", UCID-19159 (1981).
12. P. Poulsen et. al., " Negative Potential Operation of TMX-Upgrade ", UCID-19341 (1982).
13. J. A. Byers, private communication.
14. R. J. Mason, Phys. Fluids **14** ,1943 (1971).
15. C. K. Birdsall and A. B. Langdon , Plasma Physics Via Computer Simulation , McGraw-Hill, New York (1984).
16. A. V. Gurevich, Zh. Eksp. Teor. Fiz. **53** ,953 (1967). [Sov. Phys. JETP **26** (3),575 (1968).]
17 A. B. Langdon, private communication
18 R. W. Hockney and J. W. Eastwood, *Computer Simulation Using Particles* , McGraw-Hill (1981).